European Journal of Medicinal Chemistry 207 (2020) 112743

Contents lists available at ScienceDirect

European Journal of Medicinal Chemistry

journal homepage: http://www.elsevier.com/locate/ejmech

Research paper

Rational design of new multitarget histamine H_3 receptor ligands as potential candidates for treatment of Alzheimer's disease

Dorota Łażewska [a, *], Marek Bajda [b], Maria Kaleta [a], Paula Zaręba [b], Agata Doroz-Płonka [a], Agata Siwek [c], Alaa Alachkar [d], Szczepan Mogilski [e], Ali Saad [d], Kamil Kuder [a], Agnieszka Olejarz-Maciej [a], Justyna Godyń [b], Dorota Stary [b], Sylwia Sudoł [a], Małgorzata Więcek [a], Gniewomir Latacz [a], Maria Walczak [f], Jadwiga Handzlik [a], Bassem Sadek [d], Barbara Malawska [b], Katarzyna Kieć-Kononowicz [a]

[a] Department of Technology and Biotechnology of Drugs, Jagiellonian University Medical College, Medyczna Str. 9, 30-688, Kraków, Poland
[b] Department of Physicochemical Drug Analysis, Jagiellonian University Medical College, Medyczna Str. 9, 30-688, Kraków, Poland
[c] Department of Pharmacobiology, Faculty of Pharmacy, Jagiellonian University Medical College, Medyczna Str. 9, 30-688, Kraków, Poland
[d] Department of Pharmacology & Therapeutics, College of Medicine and Health Sciences, United Arab Emirates University, P.O. Box 1766, Al Ain, United Arab Emirates
[e] Department of Pharmacodynamic, Faculty of Pharmacy, Jagiellonian University Medical College, Medyczna Str. 9, 30-688, Kraków, Poland
[f] Department of Toxicology, Faculty of Pharmacy, Jagiellonian University Medical College, Medyczna Str 9, 30-688, Kraków, Poland

ARTICLE INFO

Article history:
Received 23 May 2020
Received in revised form
26 July 2020
Accepted 26 July 2020
Available online 21 August 2020

Keywords:
Xanthone derivatives
Multitarget-directed ligands
Alzheimer's disease
Histamine H_3 receptor
Cholinesterase inhibitors
Monoamine oxidase inhibitors

ABSTRACT

Design and development of multitarget-directed ligands (MTDLs) has become a very important approach in the search of new therapies for Alzheimer's disease (AD). In our present research, a number of xanthone derivatives were first designed using a pharmacophore model for histamine H_3 receptor (H_3R) antagonists/inverse agonists, and virtual docking was then performed for the enzyme acetylcholinesterase. Next, 23 compounds were synthesised and evaluated *in vitro* for human H_3R (hH_3R) affinity and inhibitory activity on cholinesterases. Most of the target compounds showed hH_3R affinities in nanomolar range and exhibited cholinesterase inhibitory activity with IC_{50} values in submicromolar range. Furthermore, the inhibitory effects of monoamine oxidases (MAO) A and B were investigated. The results showed low micromolar and selective human MAO B (*h*MAO B) inhibition. Two azepane derivatives, namely **23** (2-(5-(azepan-1-yl)pentyloxy)-9H-xanthen-9-one) and **25** (2-(5-(azepan-1-yl)pentyloxy)-7-chloro-9*H*-xanthen-9-one), were especially very promising and showed high affinity for hH_3R (K_i = 170 nM and 100 nM respectively) and high inhibitory activity for acetylcholinesterase (IC_{50} = 180 nM and 136 nM respectively). Moreover, these compounds showed moderate inhibitory activity for butyrylcholinesterase (IC_{50} = 880 nM and 394 nM respectively) and *h*MAO B (IC_{50} = 775 nM and 897 nM respectively). Furthermore, molecular docking studies were performed for hH_3R, human cholinesterases and *h*MAO B to describe the mode of interactions with these biological targets. Next, the two most promising compounds **23** and **25** were selected for *in vivo* studies. The results showed significant memory-enhancing effect of compound **23** in dizocilpine-induced amnesia in rats in two tests: step-through inhibitory avoidance paradigm (SIAP) and transfer latency paradigm time (TLPT). In addition, favourable analgesic effects of compound **23** were observed in neuropathic pain models. Therefore, compound **23** is a particularly promising structure for further design of new MTDLs for AD.

1. Introduction

In the drug discovery process, the development of novel agents with potential interactions with multiple therapeutic targets is of prime importance in the field of multifactorial diseases, e.g. Alzheimer's disease (AD) [1]. Designing a new drug molecule plays a

* Corresponding author.
E-mail address: dlazewska@cm-uj.krakow.pl (D. Łażewska).

https://doi.org/10.1016/j.ejmech.2020.112743

very important role in the search for new effective therapeutic agents. Conventionally, promising lead identification is achieved by experimental high-throughput screening, but it is a time-consuming and expensive process [1,2]. Previous experimental studies have revealed that rational drug design significantly reduces the costs associated with synthesis accompanied with an increased probability that the emerged structures will be recognised as drugs. Thus far, most of the drugs available in the market were found by chance or coincidence. The current drug discovery approach includes, among others, strategies based on structure design, as structure-based drug design is becoming an essential tool for faster and more cost-efficient lead discovery relative to the traditional methods, and is especially important for diseases with complicated aetiologies such as cancer, inflammation, metabolic syndrome, and neurodegenerative and cardiovascular diseases. Accordingly, drugs with the capability to simultaneously act on several biological cells are seen as potential candidates with a high probability for their successful treatment. However, designing such compounds is quite challenging, including proper selection of biological targets, achievement of a satisfactory activity level towards these multiple targets and optimisation of their pharmacokinetic parameters [3].

AD is a neurodegenerative disorder with yet unclear aetiology. Various factors (genetic, environmental and endogenous) have been suggested to play a role in its pathogenesis and development [4].

In AD, cognitive impairments and memory loss are related to changes in many neurotransmitter systems, especially progressive damage of cholinergic neural transmission and reduction of acetylcholine level. Moreover, acetylcholinesterase (AChE) and butyrylcholinesterase (BuChE), which are hydrolysing enzymes of acetylcholine, are involved in the formation of a complex with β-amyloid and hyperphosphorylated tau protein. The accumulation of β-amyloid deposits and neurofibrillary tangles of phosphorylated tau protein in the brain tissue is also an important factor in the development of AD [4]. Moreover, literature describes that monoamine oxidase (MAO) B activity is increased in the brain of AD patients [5]. Furthermore, recent studies revealed that MAO B levels are increased both in astrocytes and neurons, and suggested that MAO B regulates β-amyloid production *via* γ-secretase [6]. The risk of AD and other forms of dementia increases with the age the same as development of pain. AD patients suffer very often not only from chronic pain, but other types as neuropathic and nociceptive are also observed [7,8]. Proper pain control in AD is difficult as pain is usually communicated orally and verbal communication deteriorates in elders.

The current cure for AD includes mostly inhibitors of acetylcholinesterase, namely donepezil, rivastigmine, and galantamine [4]. Their action mainly involves alleviating and slowing down the course of the disease without the possibility of its effective treatment or prevention. Therefore, it is advisable to search for new drugs, especially drugs that can influence multiple targets associated with AD. Consequently, multitarget-directed ligands (MTDLs) is a promising approach in the search for novel and effective anti-AD drugs.

Histamine H_3 receptors (H_3Rs) have received considerable interest in the past several years because of their distribution mainly in the central nervous system and especially in brain regions related to memory [9]. Inhibition of the activity of these receptors causes an increase in the levels of histamine and other neurotransmitters, including acetylcholine and dopamine [9].

Pharmacological studies have suggested the use of histamine H_3R antagonists/inverse agonists in the treatment of various human disorders, e.g. AD, Attention Deficit Hyperactivity Disorder (ADHD), Parkinson's disease, schizophrenia, narcolepsy and allergy [10]. Recently also promising analgesic effects of histamine H_3R ligands was shown [11]. In the past years, in addition to selective H_3R antagonists/inverse agonists, multitarget (mostly dual acting) ligands were also obtained. Compounds were designed as structures exhibiting antagonism/inverse agonism towards H_3Rs while simultaneously affecting other biological targets [12,13]. Some of the promising structures, namely **UW-MD-71** and **E244**, with dual activity of H_3Rs antagonism and cholinesterase inhibition are shown in Fig. 1 [14–16]. Recently, another propitious multitarget compound, namely **contilisant** (Fig. 1), was reported to show human H_3Rs ($h$$H_3$Rs) antagonism, cholinesterases and monoamine oxidases (MAO) A and B inhibition and sigma 1 receptor agonism [17,18].

Xanthones (dibenzo-γ-pyrones) are compounds broadly distributed in nature and exhibit a wide variety of pharmacological activities, e.g. antibacterial, anti-inflammatory, antitumoral, glucosidase inhibitory, and cardioprotective [19–22]. One of the derivatives, namely compound DMXAA (Vadimezan, (5,6-dimethyl-9-oxo-9*H*-xanthen-4-yl)-acetic acid), has reached the stage of clinical trials as a tumour-vascular disrupting agent but failed in the phase III trial [23]. Recently, some other xanthones as potential ligands to treat AD were reported to show inhibition of cholinesterases, MAO and β-amyloid aggregation as well as antioxidant activity [24–26]. Structures of some promising xanthones with cholinesterase inhibitory activity are shown in Fig. 2 [25,26].

On the basis of these literature data and to continue our previous studies in this field [16,27,28], we designed new structures as potential multifunctional ligands for the treatment of AD. Xanthone-containing compounds were designed on the basis of the structure of **pitolisant** (the first H_3R ligand that entered the market as Wakix® [29]) and a xanthone derivative **1** with anticholinesterase activity (Fig. 3). Compound **1** showed structural elements that according to the proposed general construction pattern of histamine H_3R antagonists/inverse agonists should be in a molecule: a tertiary basic amine connected *via* a linker (commonly a linear chain) to the "eastern" arbitrary fragment [30] (see Fig. 3).

Considering these similarities, we initially designed six xanthones (Table 1S, supplementary data) and performed molecular docking to AChE [16]. The obtained results showed high ChemScore values ($47 < \text{Score} < 51$) for these compounds (Table 1S, supplementary data). Moreover, we evaluated *in silico* drug-likeness (Table 1S, supplementary data) of compounds using the SwissADME web tool and obtained promising molecular properties of these compounds [31]. Thus, encouraged by these results, we designed and synthesised (Scheme 1) the entire series of xanthones (**6**–**28**) and tested these compounds in *in vitro* assays to evaluate their $h$$H_3$R affinity and cholinesterase inhibitory activity. The binding mode of the obtained compounds with AChE and BuChE was studied by docking to the enzyme active sites (acetylcholinesterase PDB code: 1EVE; butyrylcholinesterase PDB code: 1P0I). Moreover, as molecular docking into the active site of human MAO B (hMAO B) showed promising results, all compounds were tested for hMAO A and hMAO B inhibitory activity. Furthermore, molecular docking studies were performed for histamine H_3R. Next, the two most promising compounds were selected for *in vivo* studies to evaluate their procognitive and analgesic properties. In addition the membrane permeability of these compounds was tested *in vitro*.

2. Results and discussion

2.1. Chemistry

A series of 2-(cycloaminoalkoxy)xanthones was obtained by the multistep process as shown in Scheme 1. First, 2-hydroxyxanthone

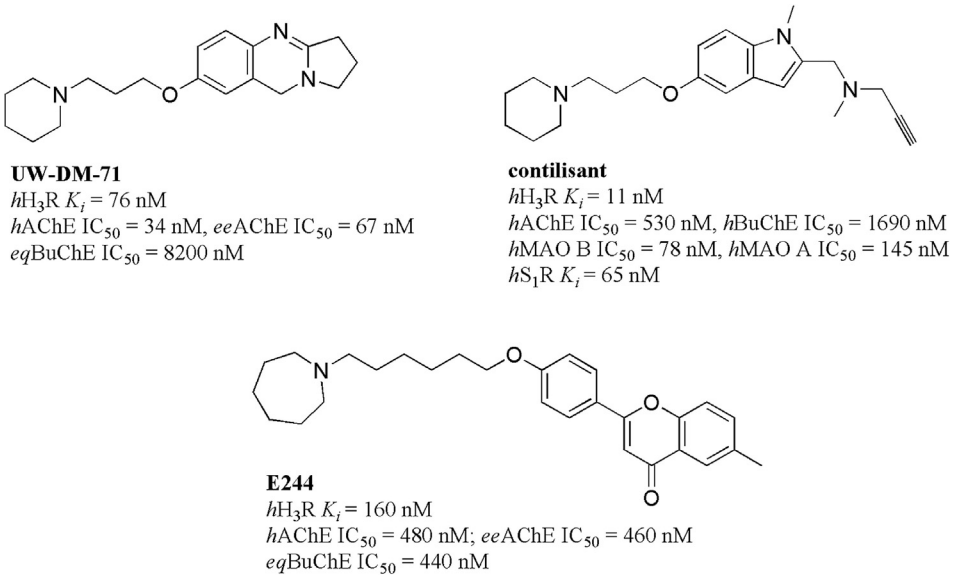

Fig. 1. Structures of histamine H_3 receptor ligands with multitarget activities. *ee*AChE – AChE from *electric eel*; *eq*BuChE- BuChE from *equine serum*. Data from Ref: **UW-DM-71** [14]; **E244** [16]; **contilisant** [17,18].

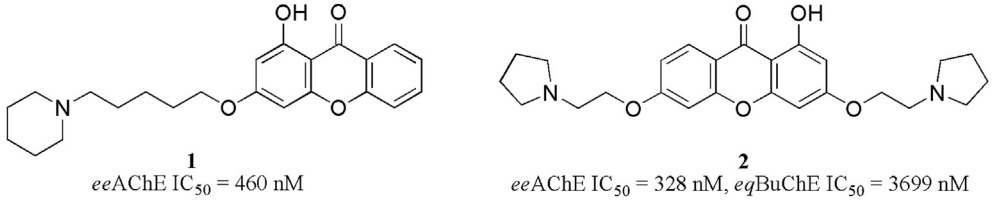

Fig. 2. Structures and cholinesterase inhibitory activity of xanthone derivatives. *ee*AChE – AChE from *electric eel*; *eq*BuChE- BuChE from *equine serum*. Data from Ref: **1** [25]; **2** [26].

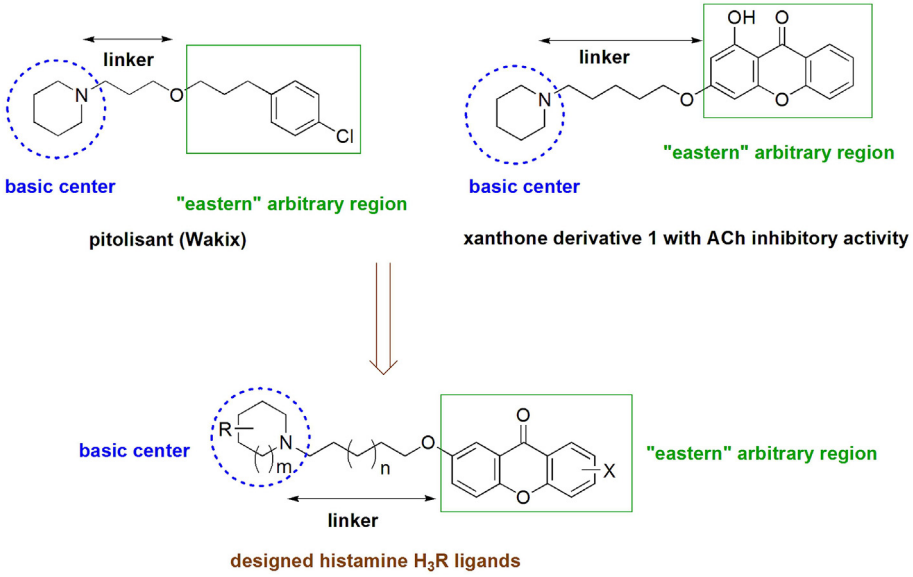

Fig. 3. Structure of **pitolisant**, xanthone derivative **1** and designed compounds showing the pharmacophore features for histamine H_3 receptor antagonist/inverse agonists.

or 6 (7)-chloro-2-hydroxyxanthone was prepared by coupling of a proper 2-chlorobenzoic acid with 4-methoxyphenol by Ullmann condensation followed by cyclisation and demethylation of 2-(4-methoxyphenoxy) acid in concentrated sulfuric acid [32]. Then, *O*-alkylation with α,ω-dibromoalkanes was performed in an aqueous solution of sodium hydroxide. The final compounds were synthesised by amination of 2-(bromoalkoxy)xanthones with an appropriate amine (piperidines or azepane) in the mixture of ethanol:water (21:4) as described previously [33]. Oily products were converted to oxalate salts by reaction with oxalic acid.

Table 1
Biological activity of synthesized compounds (**6**–**28**).

Compound	hH$_3$R[a] K_i ± SEM [nM]	*ee*AChE[b]	*eq*BuChE[c]	hMAO B[d]	hMAO A[d]
		IC_{50} ± SEM [nM]	IC_{50} ± SEM [nM]	IC_{50} ± SEM [nM]	%Inh. at 1 μM[e]
6	172 ± 3	622 ± 9	2540 ± 42	1498 ± 314	6%
7	150 ± 11	238 ± 4	983 ± 24	756 ± 154	5%
8	1060 ± 21	358 ± 6	2000 ± 67	939 ± 81	4%
9	203 ± 6	378 ± 8	1983 ± 50	946 ± 88	8%
10	282 ± 21	620 ± 1	954 ± 23	1821 ± 195	8%
11	156 ± 8	342 ± 4	978 ± 24	4205 ± 966	1%
12	56 ± 2	353 ± 8	2829 ± 89	1980 ± 299	11%
13	148 ± 3	691 ± 1	685 ± 13	665 ± 119	2%
14	100 ± 8	387 ± 7	1150 ± 28	1548 ± 23	4%
15	1105 ± 51	384 ± 9	2040 ± 51	1830 ± 285	42%
16	436 ± 5	307 ± 5	1470 ± 32	717 ± 81	28%
17	110 ± 8	697 ± 16	1090 ± 30	1864 ± 18	1%
18	448 ± 57	421 ± 5	1610 ± 32	1538 ± 446	22%
19	140 ± 11	386 ± 5	1100 ± 27	673 ± 44	5%
20	97 ± 8	406 ± 7	965 ± 18	856 ± 205	6%
21	520 ± 31	561 ± 11	1510 ± 41	1642 ± 578	37%
22	465 ± 41	525 ± 8	899 ± 23	720 ± 119	28%
23	170 ± 10	180 ± 3	880 ± 26	775 ± 111	4%
24	86 ± 5	314 ± 4	1280 ± 34	2111 ± 467	2%
25	100 ± 1	136 ± 10	394 ± 6	897 ± 150	12%
26	496 ± 23	308 ± 6	605 ± 10	385 ± 2	3%
27	602 ± 11	235 ± 5	1240 ± 30	975 ± 246	5%
28	238 ± 25	270 ± 5	545 ± 10	1387 ± 237	23%
pitolisant	30 ± 4 12 ± 3[i]	(3.0%)[f,g]	8400 ± 180	(2%)[h]	9%
tacrine		32 ± 2[g]	1.5 ± 0.5[g]	nt[j]	nt[j]
rasagiline	nt[j]	nt[j]	nt[j]	25 ± 7	nt[j]
safinamide	nt[j]	nt[j]	nt[j]	8 ± 1	nt[j]
clorgiline	nt[j]	nt[j]	nt[j]	nt[j]	1.8 ± 0.5

[a] [^{3}H] N^{α}-Methylhistamine binding assay performed with cell membrane preparation of CHO−K1 cells stably expressing the human H_3 receptor; mean value of two independent experiments ± SEM.
[b] AChE from *electric eel*; IC_{50}, mean value for three experiments.
[c] BuChE from *equine serum*; IC_{50}, mean value for three experiments.
[d] Fluorometric Amplex™ Red MAO assay.
[e] %Inhibition of hMAO A at 1 μM; mean values of two independent experiments.
[f] %Inhibition of *ee*AChE at 10 μM.
[g] Data from Ref. [16].
[h] %Inhibition of hMAO B at 1 μM; mean values of two independent experiments.
[i] Data from Ref. [35].
[j] Not tested.

Compounds were characterised by spectral analysis (^{1}H NMR and/or ^{13}C NMR and/or IR), mass spectrometry (MS) and elemental analysis.

2.2. Human histamine H_3 receptor affinity

All tested compounds showed affinity for hH$_3$R in submicromolar range. The K_i values varied between compounds from good ($K_i = 56$ nM; **12**) to weak ($K_i = 1105$ nM; **15**). Most compounds showed moderate hH$_3$R affinities (K_i: 100−500 nM). The results are summarised in Table 1. Both the most potent and the least active hH$_3$R ligands were derivatives of 3-methylpiperidine (**12** and **15**). Generally, 3-methylpiperidine (**11**–**16**) and azepane derivatives (**23**–**28**) were among the most potent compounds, whereas 4-methylpiperidine derivatives (except **20**) were the weakest ligands. The introduction of a chlorine substituent into the xanthone moiety (6- or 7-position) did not influence hH$_3$R affinity. In the pentyl derivatives series (**7**, **12**, **13**, **18**, **19**, **24** and **25**), the better was the 6-position, while in the hexyl series (**9**, **10**, **15**, **16**, **21**, **22**, **27** and **28**), the more potent were derivatives with the 7-chlorine substituent. Elongation of the carbon chain from five to six atoms influenced hH$_3$R affinity. Almost all (except **20**) the most potent hH$_3$R ligands ($K_i < 100$ nM) were pentyl derivatives. Furthermore, in most cases, the hexyl-linked xanthones were less potent than their pentyl analogues, e.g. **15** vs **12**, **27** vs **24**. Thus, carbon chain elongation from five to six atoms appeared unprofitable for hH$_3$R affinity. These results are consistent with our previous studies [34].

2.3. Cholinesterase inhibitory activity

Compounds were tested for acetyl- and butyrylcholinesterase inhibition using the slightly modified method established by Ellman et al. with commercial tacrine as the reference standard [36]. Inhibitory activity was determined against AChE from *electric eel* (*Electrophorus electricus*, *ee*AChE) and BuChE from *equine serum* (*eq*BuChE). All tested compounds exhibited cholinesterase inhibition with IC_{50} values in (sub)micromolar range. Generally, compounds showed higher AChE inhibition (136 nM $\leq IC_{50} \leq$ 697 nM) than BuChE inhibition (394 nM $\leq IC_{50} \leq$ 2829 nM). The most potent *ee*AChE inhibitors were compounds **23** and **25** with the five-carbon linker and an azepane moiety, and with IC_{50} values of 180 nM and 136 nM respectively. Generally, all azepane derivatives (**23**–**28**) were among the most potent AChE inhibitors. The same tendency was noted in BuChE inhibition. No correlation was observed between the change of carbon length (five to six) or the position of chlorine substituent (6- or 7-) in the xanthone ring and inhibition of cholinesterase activity.

Two compounds **23** and **25** with the highest *ee*AChE inhibitory potencies ($IC_{50} \leq 180$ nM) were chosen for the inhibition of human AChE (*h*AChE) and human BuChE (*h*BuChE). Tacrine and donepezil

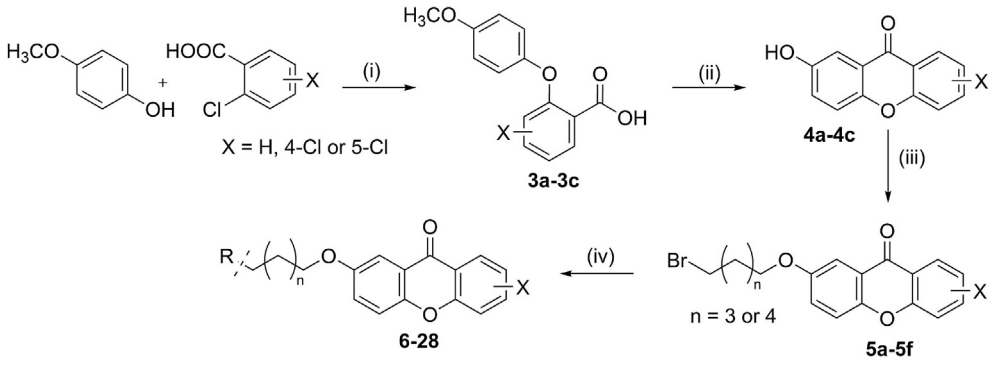

Compound	R	n	X	Compound	R	n	X
6		3	H	**17**		3	H
-		-	-	**18**		3	6-Cl
7		3	7-Cl	**19**		3	7-Cl
8		4	H	**20**		4	H
9		4	6-Cl	**21**		4	6-Cl
10		4	7-Cl	**22**		4	7-Cl
11		3	H	**23**		3	H
12		3	6-Cl	**24**		3	6-Cl
13		3	7-Cl	**25**		3	7-Cl
14		4	H	**26**		4	H
15		4	6-Cl	**27**		4	6-Cl
16		4	7-Cl	**28**		4	7-Cl

Scheme 1. Synthesis way of designed compounds. (i) CH_3ONa, Cu_2O/Cu, oil, 195–200 °C, 5 h; (ii) concentrated H_2SO_4, reflux, 48 h; (iii), $BrCH_2(CH_2)_nCH_2Br$, K_2CO_3, KI, acetone, reflux, 10–12 h; (iv) amine, K_2CO_3, KI, ethanol:water (21:4), reflux 12–24 h.

were included as reference compounds. The results (Table 2) confirmed high inhibitory effects of both compounds for *h*AChE. IC_{50} values were comparable (especially for **25**) with the data obtained from *ee*AChE for **23** and **25** (**25**: *h*AChE IC_{50} = 120 nM vs *ee*AChE IC_{50} = 136 nM; **23**: *h*AChE IC_{50} = 392 nM vs *ee*AChE IC_{50} = 180 nM). Moreover, compound **25** showed *h*AChE inhibition with the similar strength as the reference compound tacrine (IC_{50} = 131 nM). However, the results obtained for *h*BuChE show weaker inhibitory activity than that for *eq*BuChE (e.g. **25**: *h*BuChE IC_{50} = 1595 nM vs *eq*BuChE IC_{50} = 394 nM).

2.4. Kinetic studies of cholinesterases for selected compounds

Because of the highest potency towards *ee*AChE, **23** and **25** were selected as representatives for kinetic studies for both enzymes (*ee*AChE and *eq*BuChE) to investigate the mechanism of inhibition. Analysis of the Lineweaver-Burk reciprocal plots (1/V vs 1/S) showed that compounds **23** and **25** (Figs. 4A and 5A) displayed linear noncompetitive inhibition, as increased slopes and preserved intercepts at increasing concentrations of the inhibitor were observed for both enzymes. Noncompetitive type of inhibition was further confirmed by Cornish–Bowden plots (S/V vs I) (Figs. 4B and 5B).

Table 2
Human acetyl- and butyrylcholinesterase inhibitory activity of selected compounds.

Compound	human AChE IC_{50} nM ± SEM	human BuChE IC_{50} nM ± SEM
23	392 ± 11	1278 ± 29
25	120 ± 2	1595 ± 53
tacrine	131 ± 2	34 ± 0.3
donepezil	6 ± 0.1	nt[a]

[a] Not tested.

2.5. MAO A and B inhibition

MAO A and B inhibitory effects were evaluated using Amplex Red Monoamine Oxidase kits [37]. Rasagiline (MAO B), safinamide (MAO B) and clorgiline (MAO A) were used as reference compounds. Initially, all synthesised compounds were tested at the concentration of 1 μM for *h*MAO B and at the concentrations of 10 μM (first; data not shown) and 1 μM (next) for *h*MAO A. All compounds that showed more than 50% of inhibition activity at the concentration of 1 μM were further evaluated, and their IC_{50} values were determined. The results are outlined in Table 1. Most compounds showed moderate to weak inhibition of *h*MAO B (IC_{50} > 380 nM), whereas none of the tested compounds displayed higher than 50% inhibition potency against *h*MAO A at the concentration of 1 μM. According to these results, the tested compounds showed better inhibition profile against *h*MAO B than against *h*MAO A. The most potent *h*MAO B inhibitor was compound **26** with an azepane moiety and IC_{50} of 385 nM. Among (un) substituted piperidines (**6**–**22**), especially in the pentyl series (**6**, **7**, **11**–**13** and **17**–**19**), the introduction of 7-chlorine substituent increased the inhibitory activity towards *h*MAO B in comparison with unsubstituted or 6-Cl substituted compounds (**7** vs 6; **13** vs **11** vs **12** or **19** vs **17** vs **18**). However, such correlation was not seen in azepane's series (**23**–**28**).

2.6. Molecular docking to histamine H_3 receptor

Among the four histamine receptors reported to date, crystal structure for only histamine H_1 receptor has been resolved (PDB ID: 3RZE [38]). Therefore, in search for novel histamine H_3R ligands, homology modeling methods are used. In the present study, a histamine H_3R homology model was used to build crystal structure of M_2 muscarinic acetylcholine receptor (PDB ID: 3UON) with the

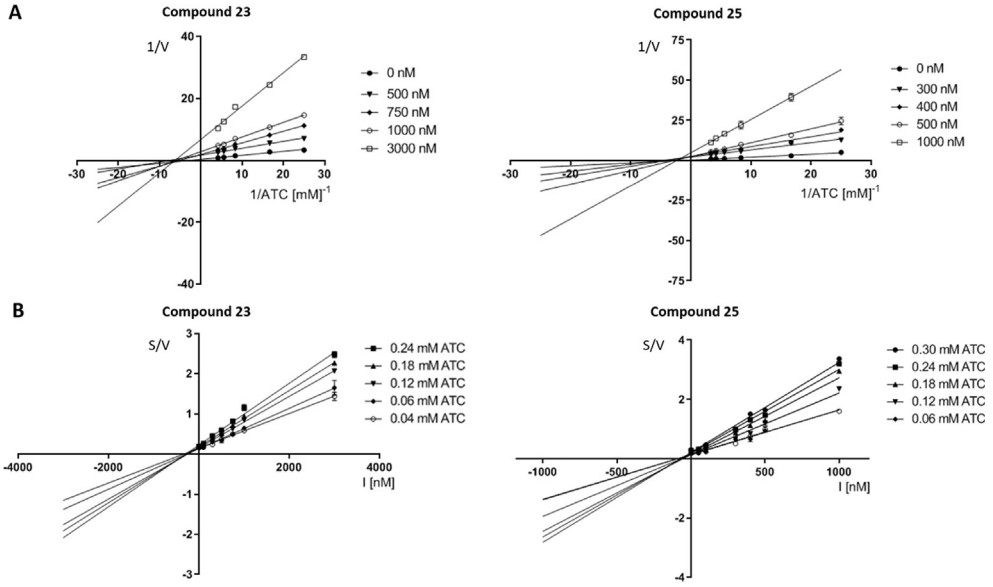

Fig. 4. Lineweaver-Burk (A) and Cornish-Bowden (B) plots illustrating non-competitive *ee*AChE inhibition by compound **23** and **25**. S = substrate (ATC) concentration; V = initial velocity rate; I = inhibitor concentration.

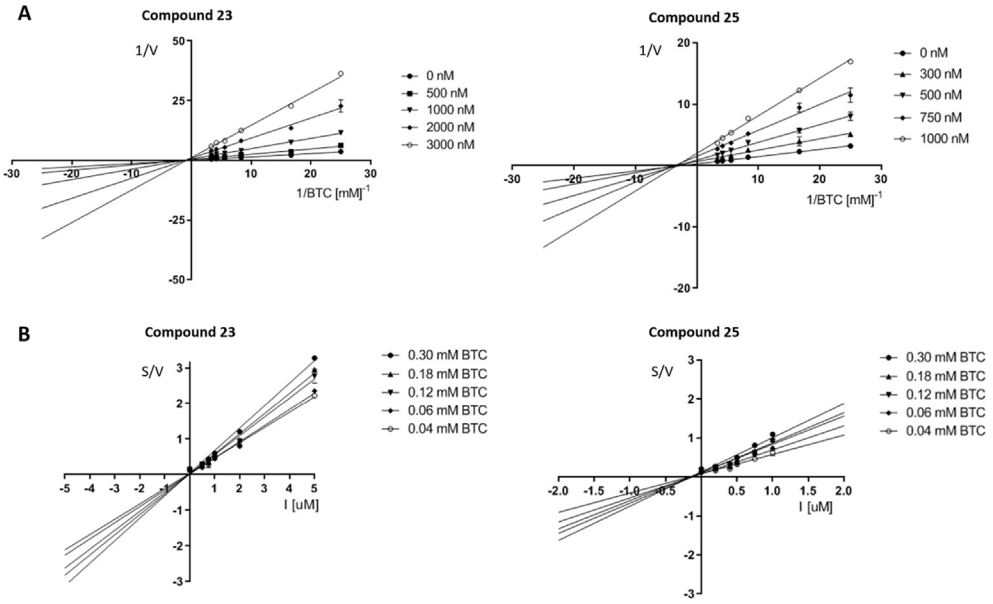

Fig. 5. Lineweaver-Burk (A) and Cornish-Bowden (B) plots illustrating non-competitive *eq*BuChE inhibition by compound **23** and **25**. S = substrate (BTC) concentration; V = initial velocity rate; I = inhibitor concentration.

reference ligand pitolisant positioned in the binding pocket, according to the data described in literature [39].

All the docked compounds were characterised by docking score values between −10.019 and −4.597. For most of them, salt bridge and/or hydrogen bond formation between protonated amine nitrogen and GLU206$^{5.46}$ was found — a supposedly key histamine H_3R antagonist/inverse agonist interaction (upper case numeration according to Balesteros–Weinstein [40]). Additionally, previously described H-bond formation between TYR374$^{6.51}$ and ether oxygen was observed (Fig. 6). The position of protonated basic moieties of the ligands was mostly fixed, independent of the alkyl linker length. A similar finding was noted for xanthone fragments – for all of the docked ligands these fragments were placed in a "hydrophobic cage" formed by PHE193 and TYR189 (ECL2), TYR94$^{2.64}$, TYR91$^{2.61}$ and TYR 394$^{7.35}$. Moreover, the latter one additionally stabilised the structures through π-π stacking. For the "meta" chlorine derivatives, additional π-π stacking with TYR94$^{2.64}$ was also present. In fact, halogen bond formation between chlorine atoms and the hydroxyl proton of TYR91$^{2.61}$ was observed despite its position in the xanthone moiety (Fig. S1; Supplementary data). On the other hand, hydrogen bond is formed between the carbonyl group and one of the nitrogen atoms of ARG381$^{6.58}$, which is in agreement of our previous findings [41].

2.7. Molecular docking to cholinesterases

2.7.1. Molecular docking to acetylcholinesterase

The docking studies for tested compounds allowed us to

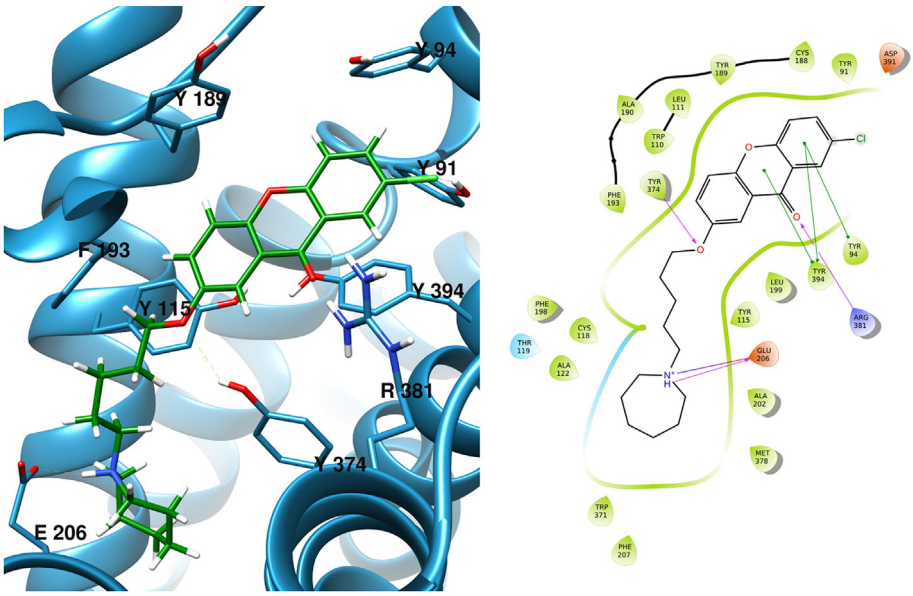

Fig. 6. Compound **25** in histamine H_3 homology receptor binding pocket (left) and its ligand-interaction diagram (right). Hydrogen bonds are represented by yellow and halogen bonds by violet dashed lines. TM5 was partly removed for better viewing purposes. (For interpretation of the references to colour in this figure legend, the reader is referred to the Web version of this article.)

describe their binding mode in the active site of acetylcholinesterase (PDB code: 1EVE). Most of them bound to the enzyme in a similar manner. The basic amines were close to the catalytic triad and anionic site residues. The alkyl chain created hydrophobic interactions within the anionic site and the acyl pocket. The xanthone moiety was located between aromatic amino acids from the peripheral anionic site [42]. The most active compounds **25** (IC_{50} = 136 nM) and **23** (IC_{50} = 180 nM) mimicked the binding mode of donepezil in the acetylcholinesterase active site [43]. Their best-ranked poses are shown in Fig. 7.

The azepane rings of both the described compounds were located between His440 from the catalytic triad and anionic site residues Trp84 and Phe330. The protonated nitrogen atoms interacted with aromatic rings through cation−π interactions. Moreover, the nitrogen atoms could form hydrogen bond interactions with water molecule (1159). Alkyl chains were responsible for hydrophobic interactions with Phe330, Phe331, and Phe290 from the anionic site and the acyl pocket of the enzyme.

For compound **25**, the oxygen atom from the ether linker formed a hydrogen bond with water 1254, and thus, it mimicked interactions of the oxygen atom from the indanone ring of donepezil. On the other hand, compound **23** was observed to form a hydrogen bond between its oxygen atom from the ether linker and the hydroxyl moiety of Tyr121 from the peripheral anionic site (PAS). In the AChE active gorge, the Tyr121 hydroxyl moiety interacted with the abovementioned water molecule 1159. This type of interaction could be associated with its potent biological activity and was observed in our previous studies [16].

Tested compounds **23** and **25** contain large dibenzo-γ-pyrone (xanthone) fragments located between PAS residues. These fragments created hydrophobic interactions with aromatic amino acids such as: Tyr334, Tyr70, Tyr121 and Trp279. Additionally, the rigid structure of xanthone enabled to create π-π stacking with Trp279. As water 1254 was important for the binding of donepezil, it was also found to interact with the carbonyl oxygen atom from xanthone of compound **23**.

2.7.2. Molecular docking to butyrylcholinesterase

The tested compounds were also docked into the active site of butyrylcholinesterase. The analysis of the binding mode with BuChE showed the most common and top-ranked poses presented in Fig. 8. The heterocyclic moiety with tertiary amine was located

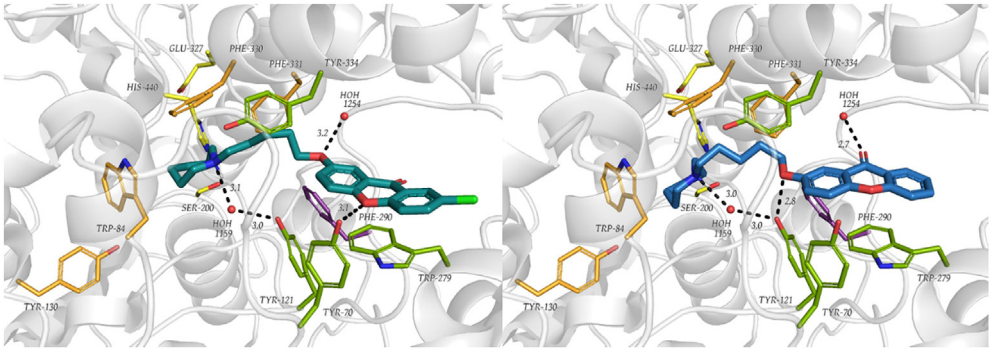

Fig. 7. Binding mode of compound **25** (left panel) and compound **23** (right panel) within the acetylcholinesterase active site. Residues coloured in: yellow − catalytic triad, orange − anionic site, green − peripheral anionic site, purple − acyl pocket. (For interpretation of the references to colour in this figure legend, the reader is referred to the Web version of this article.)

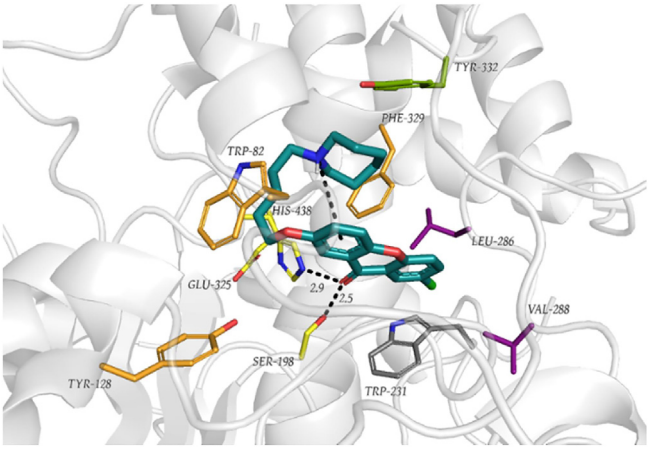

Fig. 8. Binding mode of compound **25** within butyrylcholinesterase active site. Residues coloured in: yellow – catalytic triad, orange – anionic site, green – peripheral anionic site, purple – acyl pocket. (For interpretation of the references to colour in this figure legend, the reader is referred to the Web version of this article.)

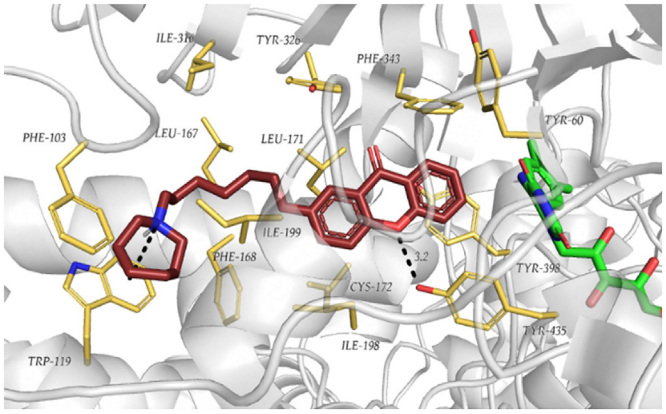

Fig. 9. Binding mode of compound **26** within human monoamine oxidase B active site. Residues coloured in yellow, green - cofactor FAD. (For interpretation of the references to colour in this figure legend, the reader is referred to the Web version of this article.)

between amino acids from PAS and the anionic site. The alkyl linker interacted with hydrophobic amino acids from the anionic site. The xanthone fragment interacted with amino acids of the catalytic triad and with the acyl pocket residues [43].

Compound **25** (IC_{50} = 394 nM) bound to the butyrylcholinesterase active site as follows: the azepane ring of the compound showed hydrophobic interactions with Tyr332 from the peripheral anionic site. A flexible five-carbon alkyl chain enabled to bend the molecule. Consequently, the protonated nitrogen atom could form cation–π interaction with the aromatic ring of xanthone. Moreover, the carbonyl oxygen atom in position 9 of the xanthone ring interacted by hydrogen bonds with amino acids from the catalytic triad: His438 and Ser198. These interactions were observed in our previous study for azepane derivatives with 6-methylchromone moiety. This H-bond network could explain the high inhibitory activity. Additionally, the aromatic ring with the chlorine substituent interacted with hydrophobic amino acids such as Phe329 and Trp231 and with branched-chain amino acids from the acyl pocket: Val288 and Leu286. This binding mode was similar in comparison with the 6-methylchromone group [16].

2.8. Molecular docking to MAO B

All the tested compounds showed a similar arrangement within the human MAO B active site (PDB code: 4A79). Heterocyclic moieties with a tertiary basic amine were located on the edge of the lipophilic pocket. The alkyl linker interacted with the enzyme through hydrophobic interactions. The dibenzo-γ-pyrone fragments were located near the cofactor (FAD). For the top-ranked poses, the calculated ChemScore values were between 49.75 and 56.37.

Fig. 9 shows the binding of **26,** the most active inhibitor of *h*MAO B (IC_{50} = 385 nM), with the enzyme active site. The azepane ring of the inhibitor interacted with hydrophobic amino acids such as Phe103, Trp119 and Ile199. Moreover, the protonated nitrogen atom could form cation-π interactions with Trp119. The alkyl chain of compound **26** created hydrophobic interactions with Ile316, Leu167, Leu171, Ile199 and Ile198. The xanthone ring was close to the FAD and formed aromatic ring interactions with the residues of Tyr326, Tyr435, Phe343, Tyr60, and Tyr398. Binding within the *h*MAO B active site was stabilised by hydrogen bonds between the oxygen atom of xanthone and the hydroxyl group of Tyr435 for tested compound **26**.

We observed significant changes in the inhibitory activity in comparison with compounds from our previous work [44]. This could be related to the differences in the binding mode. For the most active inhibitor of *h*MAO B described previously (IC_{50} = 4.5 nM), the pyrrolidine ring was close to the cofactor (FAD). This binding mode in the active site of enzyme seems to be crucial to obtain strong inhibitory activity. The differences in the potency of this series of compounds could be explained by the lack of a hydrogen bond with Tyr435. This type of interaction was not observed for structures with high IC_{50} values, such as **6**, **24** or **28**.

2.9. In vivo studies of compounds *23* and *25*

2.9.1. Analgesic effect of selected compounds

2.9.1.1. Formalin test in mice. Subcutaneous injection of formalin results in a stimulation and then damage of sensory endings. The nociceptive response of animals consists of two phases: phase I is associated with immediate activation of nociceptors and phase II leads to sensitisation of spinal reflex circuits. Moreover, it has been suggested that formalin injection results in pathological changes that resemble those observed in nerve injury and neuropathic pain [45]. In our previous studies, we showed that opioids attenuate the nociceptive response in both phases, whereas NSAIDs preferentially diminish the nociceptive response in phase II of the test [46]. Furthermore, we showed that histamine H_1 receptor, H_3R and H_4 receptor antagonists also attenuated nociceptive response, thus showing promising efficacy especially in the late phase [46–48]. The same observation was made by Hamzeh Gooshchi et al. [49] and Dou et al., [50]. In formalin-induced pain in rats, H_3R ligands like thioperamide [49] and 2-methyl-7-(3-morpholinopropoxy)-3,4-dihydroisoquinolin-1(2H)-one [50] significantly suppressed pain in the late phase. Now, as continuation of our previous studies, we investigated analgesic properties of the two most promising xanthone derivatives: **23** and **25**. As shown in Fig. 10, the intraperitoneal (*i.p.*) administration of compound **23** prior to the subcutaneous injection of formalin significantly attenuated the nociceptive response in mice in both phases of the test. Its ED_{50} value in phase I was 24.7 mg/kg, whereas the ED_{50} value in phase II was 11.3 mg/kg. Compound **23** was more effective in both phases than the second investigated compound **25** (phase I: ED_{50} = 27.3 mg/kg and phase II: ED_{50} = 22.5 mg/kg). These results suggest promising analgesic properties of compound **23**, which were subsequently confirmed in other models of pain.

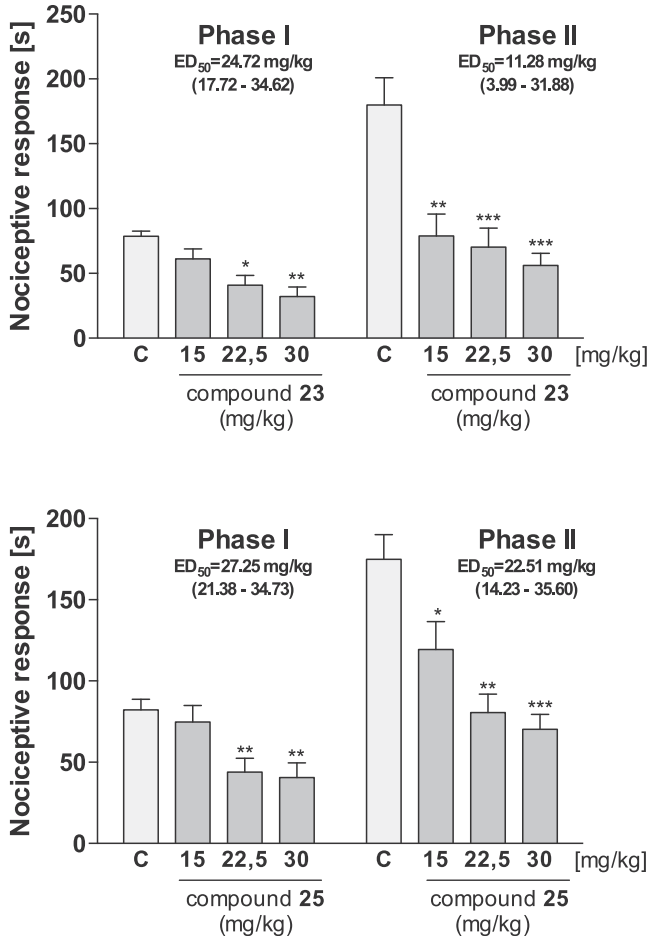

Fig. 10. Antinociceptive activity of compounds **23** and **25** in the formalin test. Results are shown as time of licking in phase I (0–5 min after intraplantar injection of formalin) and in phase II (15–30 min after formalin injection). Each value represents the mean ± S.E.M. for 8–10 animals. Statistical analysis: one-way ANOVA followed by *post hoc* Dunnett's test. Statistical significance compared to vehicle-treated animals (Tween): *p < 0.05, **p < 0.01, ***p < 0.001. C-control group.

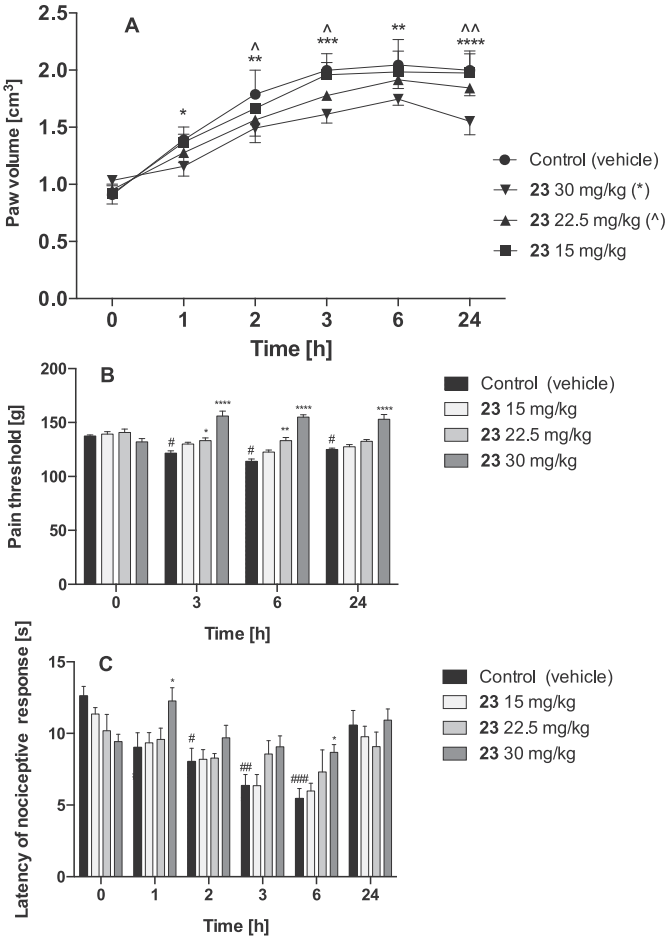

Fig. 11. Effect of compound **23** on carrageenan-induced oedema (**A**), mechanical hyperalgesia (**B**) and on thermal hyperalgesia (**C**) developed after subplantar injection of 1% carrageenan in rats. Data are expressed as means ± S.E.M. for 6 animals. 0 - the initial reaction considered as the nociceptive reaction before carrageenan administration. Statistical significance compared to vehicle-treated animals (control): *p < 0.05, **p < 0.01, ***p < 0.001, ****p < 0.0001; ^ p < 0.05, ^^ p < 0.01 (for the dose of 22.5 mg/kg). Statistical analysis: two-way ANOVA post hoc Bonferroni test. Statistical significance in different time points of control group: #p < 0.05, ##p < 0.01, ###p < 0.001. Statistical analysis: one-way ANOVA followed by Dunnett's Multiple Comparison Test.

2.9.1.2. Carageenan-induced paw oedema and mechanical and thermal hypernociception in rats. Subplantar injection of carrageenan induced oedema and mechanical and thermal hyperalgesia. Fig. 11 (panel **A**) shows the time course of rat paw oedema development in the control group and groups pretreated with compound **23**. The tested compound significantly reduced paw oedema at the doses of 22.5 mg/kg and 30 mg/kg. Pretreatment with compound **23** at the dose of 22.5 mg/kg reduced paw oedema by 36.1%, 32.8%, 26.5%, 19.37% and 22.4% at 1, 2, 3, 6 and 24 h following carrageenan injection respectively. The effect of the higher dose of 30 mg/kg was more significant (77.9%, 53.3%, 52.1%, 44.9% and 57.8% of oedema reduction respectively). Thus, as oedema is one of the most significant symptoms of inflammation, we concluded that compound **23** has some anti-inflammatory activity. Fig. 11 (panel **B**) shows that the subplantar injection of carrageenan decreased the withdrawal threshold (mechanical hyperalgesia). The reduction was 88.4%, 83.0% and 90.9% of the initial reaction at 3, 6 and 24 h respectively. Pretreatment with compound **23** inhibited mechanical inflammatory hyperalgesia as observed by an increased withdrawal threshold. The most pronounced effect (118.0% ± 9.0% of the initial reaction) was observed at the dose of 30 mg/kg 3 h after inflammation induction and was maintained for 24 h. A statistically significant effect was also observed at the dose of 22.5 mg/kg; however, it was weaker (94.6% ± 4.5%). Fig. 11 (panel **C**) shows that the subplantar injection of carrageenan-induced thermal hyperalgesia as observed by decreased latency of nociceptive response for radiant heat stimulation. The initial latency of the control group (before carrageenan injection) was 12.61 ± 0.6 s and was significantly reduced to 71.4%, 63.6%, 50.3%, 43.2% and 83.3% of the initial value at 1, 2, 3, 6 and 24 h following carrageenan injection respectively. Compound **23** was significantly active at the dose of 30 mg/kg. The initial latency in that group was 9.43 ± 0.5 s. The administration of **23** changed the values to 130.0%, 102.8%, 96.0%, 92.0% and 116.0% of the initial value at 1, 2, 3, 6 and 24 h following carrageenan injection respectively. This shows that compound **23** was able to not only attenuate inflammatory hyperalgesia but also show analgesic effect for heat stimulus.

2.9.1.3. Oxaliplatin-induced neuropathic pain in mice. To investigate the analgesic activity of compound **23** in a neuropathic pain model, we tested it in oxaliplatin (OXPT)-induced peripheral neuropathy, in which mechanical and cold allodynia results from impaired regulation of the activity of ion channels among others [51]. The

neuropathy develops within a few hours after OXPT administration, which is characterised as the early phase of neuropathic pain. The second late phase develops in few days after OXPT administration. Thus, we tested compound **23** at 3 h and 7 days post neuropathy induction. We investigated the influence of compound **23** on tactile allodynia by using the von Frey method. Three hours after the administration of OXPT, we observed a significant decrease in the value of mean force that caused paw withdrawal reaction (1.82 ± 0.05 g) (61.2% of the baseline) compared to that in non-treated animals (2.97 ± 0.04 g) (the baseline). Seven days after OXPT administration, the pain threshold was 1.94 ± 0.04 (65.3% of the baseline). The observed tactile allodynia was attenuated by compound **23**, which elevated pain sensitivity threshold in the early phase in a dose-dependent manner (Fig. 12) (2.63 ± 0.08 g, 2.69 ± 0.07 g and 2.84 ± 0.07 g at the dose of 15 mg/kg, 22.5 mg/kg and 30 mg/kg, which correspond to 88.5%, 90.6% and 95.6% of the baseline value respectively). In the late phase, the values of pain threshold were as follows: 2.55 ± 0.06 g, 2.63 ± 0.08 g and 2.98 ± 0.06 g, which correspond to 85.9%, 88.5% and 100.0% of the baseline value respectively. These results indicate that compound **23** has the potential for relieving particularly neuropathic pain (all the tested doses were significantly active) and should be further tested in that direction.

2.9.2. *Memory-enhancing effects of compounds **23** and **25***

Compounds **23** and **25** were assessed in rats with dizocilpine-induced amnesia by *i.p.* administration of the tested compounds at the dose range of 1.25–5 mg/kg. To assess the memory-enhancing effect of compounds **23** and **25**, step-through inhibitory avoidance paradigm (SIAP) in step-through passive avoidance test and transfer latency paradigm time (TLPT) in elevated plus maze (EPM) test were used.

2.9.2.1. *Memory-enhancing effects of compounds **23** and **25** in SIAP.*

To determine the procognitive effect of tested compounds **23** and **25**, 9 groups were acutely pretreated with either Saline + Saline, dizocilpine (DIZ, 0.1 mg) + Saline, DIZ (0.1 mg) + **23** (1.25 mg), DIZ (0.1 mg) + **23** (2.5 mg), DIZ (0.1 mg) + **23** (5 mg), DIZ (0.1 mg) + **25** (1.25 mg), DIZ (0.1 mg) + **25** (2.5 mg), DIZ (0.1 mg) + **25** (5 mg) and DIZ + Donepezil (DOZ, 1 mg) 30–45 min prior to the test session, and their effects on DIZ-induced memory deficits were assessed by determining the STLs to enter the dark box (Fig. 13) [15,52–58]. When injected before the retention test, statistical analysis of variance showed that acute systemic pretreatment with **23** (1.25, 2.5 and 5 mg/kg), **25** (1.25, 2.5 and 5 mg/kg) or DOZ (1 mg/kg) exhibited a significant effect on STLs [$F_{(8,54)} = 290.963$; $P < 0.001$]. As compared to the saline-treated group, subsequent post hoc analyses showed that DIZ (0.1 mg/kg) decreased STL time [$F_{(1,12)} = 1858.03$; $P < 0.001$]. In addition, tested compound **23** (1.25, 2.5 and 5 mg/kg) and DOZ (1 mg/kg) exerted significant memory-enhancing effect on STLs as compared to DIZ-treated group ([$F_{(1,12)} = 262.72$; $P < 0.001$], [$F_{(1,12)} = 118.8498597$; $P < 0.05$], [$F_{(1,12)} = 25.40$; $P < 0.05$], and [$F_{(1,12)} = 1073.05$; $P < 0.001$]) respectively (Fig. 13). The procognitive effects observed for compound **23** was dose-dependent, as the dose of 1.25 mg/kg was significantly higher than that of 2.5 mg in providing memory-enhancing effect [$F_{(1,12)} = 37.66$; $P < 0.05$] (Fig. 13). Furthermore, the memory-enhancing effect provided by the dose of 2.5 mg of **23** was significantly higher than that observed with 5 mg of the same compound [$F_{(1,12)} = 16.07$; $P < 0.05$]. Contrary to this result, compound **25** failed to provide procognitive effects when administered in the same dose range (all $P > 0.05$).

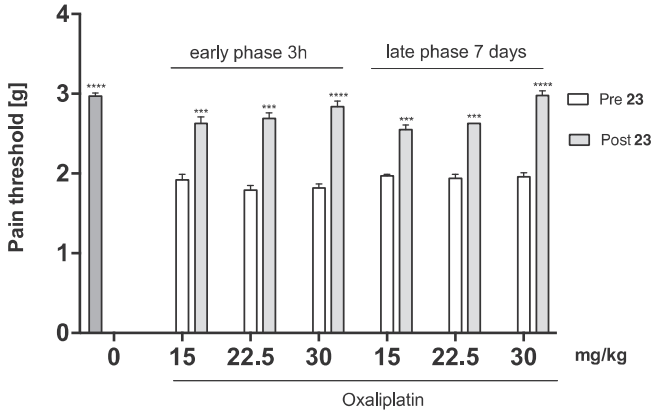

Fig. 12. Antiallodynic effects of compound **23** in the tactile allodynia evaluated in the von Frey test in oxaliplatin-induced model of peripheral neuropathy. Results compared to vehicle-treated group (Pre **23**). Statistical analysis: repeated measures analysis of variance (ANOVA), followed by Dunnett's *post hoc* comparison: ***p < 0.001, ****p < 0.0001.

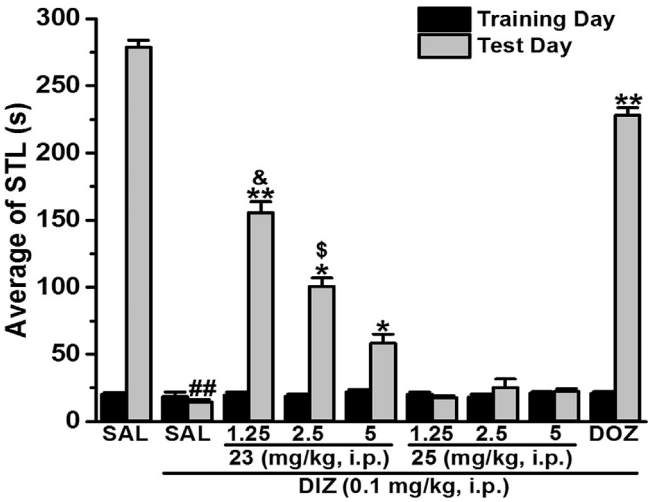

Fig. 13. Effects of compounds **23** and **25** treatment on DIZ-induced memory deficits in inhibitory avoidance paradigm. Average STL time measured on the first training day before the delivery of foot shock (black columns), and average STL time measured on the test day (grey columns). $^{\#\#}P < 0.001$ for average STL time compared with that of the SAL-treated group. $^{*}P < 0.05$ for average STLs compared with the DIZ-treated group. $^{**}P < 0.001$ for average STLs compared with the DIZ-treated group. $^{\&}P < 0.05$ for average STLs compared with the **23** (2.5 mg)-treated group. $^{\$}P < 0.05$ for average STLs compared with the **23** (5 mg)-treated group. The data are expressed as the mean ± SEM (n = 7).

2.9.2.2. *Memory-enhancing effects of compounds **23** and **25** on TLPT in the EPM test.*

The procognitive effects of tested compounds **23** and **25** on memory deficits of DIZ-treated rats in EPM paradigm were assessed in the nine treatment groups as described for SIAP. When injected before, on the test day, statistical analysis of variance showed that acute systemic pretreatment with **23** (1.25, 2.5 and 5 mg/kg), **25** (1.25, 2.5 and 5 mg/kg) or DOZ (1 mg/kg) exhibited a significant effect on TLT [$F_{(8,54)} = 5.35$; $P < 0.001$]. Further subsequent *post hoc* analyses indicated that DIZ-treated rats exhibited significantly increased transfer latency time (TLT) time when compared with control SAL-treated rats [$F_{(1,12)} = 10.28$; $P < 0.01$] (Fig. 14). Moreover, the results showed that acute systemic pretreatment with compound **23** (1.25, 2.5 and 5 mg/kg, *i.p.*) and DOZ (1 mg/kg) counteracted memory impairment of DIZ-treated animals by significantly decreasing TLT ([$F_{(1,10)} = 14.20$; $P < 0.05$], [$F_{(1,10)} = 14.20$; $P < 0.05$], [$F_{(1,10)} = 14.20$; $P < 0.05$], and [$F_{(1,10)} = 14.20$; $P < 0.05$]) respectively as compared to that in DIZ-

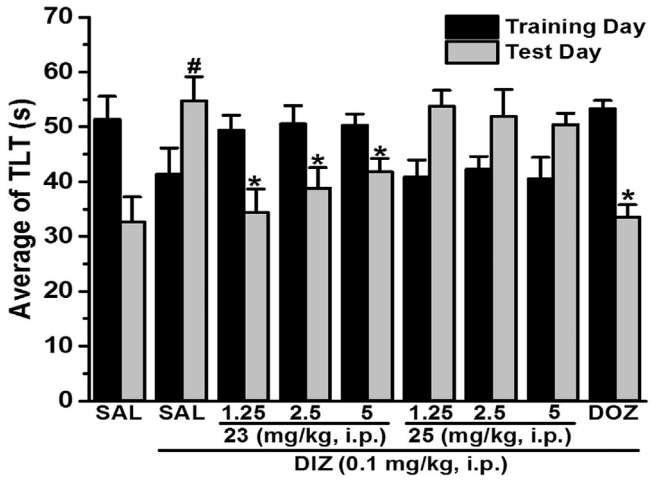

Fig. 14. Effects of compounds **23** and **25** treatment on DIZ-induced memory deficits in elevated plus maze test. Average of TLT measured on the first training day (black columns), and average of TLT measured on the test day (grey columns), namely 24 h after the training day, and 30–45 min after DIZ or tested compounds injection. $^{\#}P < 0.01$ vs saline-treated group. $^{*}P < 0.05$ vs DIZ-treated rats. Values are expressed as the mean +SEM (n = 7).

treated rats, and no significant difference was observed in the procognitive effect provided by compound **23** (1.25, 2.5 and 5 mg/kg) (all $P > 0.05$) (Fig. 14). However, compound **25** failed to attenuate the impaired memory of DIZ-treated rats (all $P > 0.05$).

On the basis of the results obtained for the *in vivo* memory-enhancing assessments, it can be concluded that acute systemic pretreatment with compound **23** significantly mitigated the memory deficits associated with systemic administration of DIZ in two different *in vivo* test models (Figs. 13 and 14). The memory-enhancing effects observed for the novel H_3R ligand **23** were consistent with earlier studies in which nonimidazole-based H_3R antagonists showed procognitive effects in rats [52–54,57]. However, compound **25** failed to attenuate the memory deficits in the same sets of behavioural experiments.

2.10. Studies on drug-likeness of compounds *23* and *25*

Taking into consideration a very similar pharmacological profile *in vitro* together with very little structural dissimilarity between **23** and **25**, the apparent discrepancy for both compounds in the pharmacological action *in vivo* is an intriguing question. The only structural difference for the compounds is seen in the presence (**25**) or absence (**23**) of chlorine substituent at the aromatic ring. This suggests the important role for hydrophobicity that is responsible for drug-like ADME properties of compounds, in particular, those associated with membrane penetration. Thus, drug-likeness studies, with special accent on membrane permeability for compounds **23** and **25,** were performed in search for a reason of the activity difference.

2.10.1. In silico ADMET and drug-likeness properties

ADMET properties of were calculated for all synthesised compounds using a free accessible web tool: SwissADME [31,59]. The calculated data are shown in Tables S2 and S3 (supplementary data). All compounds exhibited good physicochemical properties, except slightly high predicted lipophilicity (log P in the range of 4.57–5.53). SwissADME estimates drug-likeness based on five commonly used rules (Lipiński, Ghose, Veber, Egan and Muegge) to filter molecules. All compounds satisfied the rules of Lipiński and Veber. A few compounds showed one violation in Ghose's (compounds **9**, **10**, **15**, **16**, **21**, **22**, **27** and **28**) and Egan's (**15**, **16**, **21**, **22**, **27** and **28**) rule. None of the compounds complied with the rule of Muegge (one violation). Violation of only one rule does not exclude the chance of a molecule to become a drug. Moreover, according to the results, all compounds should cross the blood-brain barrier, be absorbed through the intestine and be transported by P-glycoproteins. Toxicity of the designed compounds was evaluated using ProToxII tool [60]. The programme predicted (Table S4; supplementary data) high doses of oral toxicity (LD50 > 244 mg/kg) and potential toxic behaviour to immune system (due to immunotoxicity). Further, the SwissADME programme [31,59] determined that compounds **6**–**28** should have no pan-assay interference liability (PAINS). It is worth to underline that apart from generally similar and beneficial ADMET properties for both compounds **23** and **25**, the active *in vivo* compound **23** displayed log P lower than the inactive **25**, and thus closer to the advised values for drug-likeness compounds.

2.10.2. Permeability of BBB of compounds *23* and *25*

In order to explain the differences in *in vivo* activity of compounds **23** and **25** the ability of these compounds to cross blood brain barrier (BBB) was checked using PAMPA. PAMPA is widely known experimental method for an estimation of compound's biological membrane permeability, including BBB penetration *via* passive transport. The artificial membrane imitates barriers for ligand absorption with a good correlation to *in vivo* conditions. The study was performed in accordance to the previously described method [61]. According to the manufacturer's guidelines, compounds can be classified as permeable if $P_e \geq 1.5 \times 10^{-6}$ cm/s [62]. Caffeine was used as the highly permeable reference drug. Results indicated that both tested compounds were permeable, but displayed a lower (**23**; $P_e = 5.6 \times 10^{-6}$ cm/s) or much lower (**25**; $P_e = 2.2 \times 10^{-6}$ cm/s) permeability coefficient values than that of caffeine ($P_e = 15.1 \times 10^{-6}$ cm/s; Table 3). More than twice weaker permeability of compound **25** in comparison with **23** could explain the observed difference in *in vivo* activity.

3. Conclusions

On the basis of preliminary *in silico* studies, a series of xanthone derivatives was designed, synthesised and biologically evaluated *in vitro* and *in vivo*. For the first time, xanthones are described here as MTDL with antagonistic affinities for hH_3R and inhibitory activity for cholinesterases and *h*MAO B. Most of the twenty three compounds showed affinities to both hH_3R and AChE in the nanomolar concentration range. Additionally, the compounds could also inhibit BuChE and *h*MAO B but with weaker strength than that for hH_3R and AChE. Furthermore, none of the compounds displayed any inhibitory activity towards *h*MAO A. Thus, as described here, xanthones are promising novel multifunctional agents that can improve not only cognitive symptoms of AD by hampering H_3R activity and inhibiting cholinesterases (AChE and BuChE) but also slow down the progression of AD by inhibiting *h*MAO B. In addition, *in vivo* studies showed analgesic and procognitive activity of tested

Table 3
Permeability coefficient of compounds **23** and **25**.

Compound	P_e[a,b] [10^{-6} cm/s] ± SD
23	5.6 ± 1.1
25	2.2 ± 0.3
Caffeine	15.1 ± 0.4

[a] Tested in triplicate.
[b] For permeable compounds P_e is equal or higher than 1.5 × 10^{-6}cm/s.

compounds **23** and **25**. However, in all tests, compound **23** showed the higher effect probably due to better drug-likeness properties than compound **25**, especially, membranes penetration, including BBB. Procognitive properties of **23** were comprehended in two behavioural paradigms, namely SIAP and TLPT tests, where **23** significantly ameliorated memory impairments induced by DIZ (especially at the dose of 1.25 mg/kg). In pain models (formalin test, carrageenan-induced hypernociception and oxaliplatin-induced neuropathic pain), compound **23** showed significant analgesic effect. Thus, compound **23** can be a promising lead structure in the search for MTDL for future therapeutic management of AD.

4. Experimental

4.1. Chemistry

All starting materials, reagents and solvents were obtained from commercial suppliers (Sigma Aldrich, Alfa Aesar or Chempur) and were used without further purification. Reaction progress was monitored by thin layer chromatography (TLC) on silica gel 60 F254 plates and the spots were visualized by UV light and treatment with Dragendorff reagent (solvent system: methylene chloride: methanol 9:1). Melting points (Mp) were determined using MEL-TEMP II apparatus (LD Inc. Long Beach, CA, USA) and are uncorrected. NMR (^{1}H and ^{13}C) spectra were recorded in DMSO-d_6 on Varian-Mercury-VX 300 MHz PFG (Varian, Palo Alto, CA, USA) or Avance III HD 400 MHz (Bruker; Germany) spectrometers or FT-NMR 500 MHz spectrometer (Jeol Ltd, Akishima, Tokyo, Japan). Chemical shifts (δ) are expressed in parts per million (ppm). Data are reported chemical shift, multiplicity (s, singlet; d, dublet; t, triplet; q, quartet; qu, quintet; m, multiplet; br, broad), approximate coupling constants *J* expressed in Hertz (Hz), number of protons. Recorded NMR data are available in Supplementary Materials. IR spectra were measured as KBr pellets on FT/IR Nicolet iS5 spectrometer (ThermoScientific). Mass spectra (LC/MS) were performed on Waters TQ Detector Mass Spectrometer (Water Corporation, Milford, CT, USA). Retention times (t_R) are given in minutes. UPLC/MS analysis confirmed purity (>95%) of all compounds (except **9**—93.01%, **21**—93.91% and **27**—94.98%). Elemental analyses (C, H, N) were performed on an Elemental Analyser Vario El III (Hanau, Germany) and agreed with theoretical values within ±0.4%.

4.1.1. Synthesis of starting materials

2-(4-Methoxyphenoxy)benzoic acid (**3a**). To freshly prepared sodium methoxide (100 mmol Na in 100 mL of absolute methanol) was added 2-chlorobenzoic acid (50 mmol, 7.83 g), 4-methoxyphenol (60 mmol, 7.45 g) copper (0.39 mmol, 0.025 g) and copper (I) oxide (0.17 mmol, 0.025 g) and warming on the water bath until dissolution. Then methanol was evaporated and to the rest paraffin oil (50 mL) was added and heated to 210 °C for 2 h. After cooling down paraffin oil was decanted and 50 mL od xylene was added and the precipitate was filtered, dissolved in hot water and refluxed for a few minutes with activated carbon. The filtrate was acidified with concentrated hydrochloric acid (HCl). The precipitate was crystallized with ethanol. White solid, Mp: 145—147 °C, yield 44% (5.4 g).

4-Chloro-2-(4-methoxyphenoxy)benzoic acid (**3b**). Synthesised as described for 2-(4-Methoxyphenoxy)benzoic acid from 2,4-dichlorobenzoic acid (50 mmol, 9.55 g). White solid, Mp: 200—204 °C, yield 45% (6.2 g).

5-Chloro-2-(4-methoxyphenoxy)benzoic acid (**3c**). Synthesised as described for 2-(4-methoxyphenoxy)benzoic acid from 2,5-dichlorobenzoic acid (50 mmol, 9.55 g). After acidification with concentrated hydrochloric acid as the solid did not precipitate water was decanted from oily residue and then dissolved in 50 mL of CH_2Cl_2 and purified by extraction with 1% solution of $NaHCO_3$ (twice). The inorganic solution was acidified with 10% HCl and white solid precipitate: 5.5 g, yield 39%, Mp: 115—118 °C.

2-Hydroxyxanthone (**4a**). 2-(4-methoxyphenoxy)benzoic acid (22 mmol, 5.37 g) was refluxed on the water bath with concentrated sulfuric acid (30 mL) for 2 h. Then the mixture was poured into the icy water and the formed solid was precipitated washed with water, 0.5% NaOH, water and crystallized from ethanol. Yellow solid, Mp: 235—240 °C, yield 45% (2.26 g) (Mp: 240.2—240.9 °C (ethanol) [63]).

6-Chloro-2-hydroxyxanthone (**4b**). Synthesis as 2-hydroxyxanthone from 4-chloro-2-(4-methoxyphenoxy)benzoic acid (11 mmol, 3.1 g) in 14 mL of concentrated sulfuric acid. Yellow solid, Mp: 210—218 °C, yield 32% (0.87 g).

7-Chloro-2-hydroxyxanthone (**4c**). Synthesis as 2-hydroxyxanthone from 5-chloro-2-(4-methoxyphenoxy)benzoic acid (18 mmol, 5.04 g) in 25 mL of concentrated sulfuric acid. Yellow solid, Mp: 254—250 °C, yield 85% (3.8 g).

2-(5-Bromopentyloxy)-9H-xanthen-9-one (**5a**). To the solution of 0.3 g (7.5 mmol) in 12 mL of water 2-hydroxyxanthone (**4a**) was added (7.5 mmol; 1.69 g). The mixture was stirred for a few minutes and then 1,5-dibromopentane (7.5 mmol; 1.73 g) was added and refluxed for 7 h. After cooling down the precipitate was filtered off, washed with water and purified by flash chromatography (CH_2Cl_2). Obtained white solid, Mp: 91-93 °C, yield 49% (1.34 g).

2-(5-Bromopentyloxy)-6-chloro-9H-xanthen-9-one (**5b**). Synthesis as 2-(5-bromopentyloxy)-9*H*-xanthen-9-one from 6-chloro-2-hydroxyxanthone (**4b**) (5 mmol; 1.23 g) in NaOH solution (5 mmol; 0.2 g in 10 mL of water) with 1,5- dibromopentane (5 mmol; 1.15 g). Refluxed for 5 h. After cooling down the precipitate was filtered off, washed with water and the crude product was used for the synthesis without further purification. Light yellow solid, (0.8 g). The reaction was repeated. Obtained light yellow solid (0.5 g).

2-(5-Bromopentyloxy)-7-chloro-9H-xanthen-9-one (**5c**). Synthesis as 2-(5-bromopentyloxy)-9*H*-xanthen-9-one from 7-chloro-2-hydroxyxanthone (**4c**) (6 mmol; 1.48 g) in NaOH solution (6 mmol; 0.24 g in 10 mL of water) with 1,5- dibromopentane (6 mmol; 1.38 g). Refluxed for 12 h. After cooling down the precipitate was filtered off, washed with water and the crude product was used for the synthesis without further purification. White solid (1.75 g).

2-(6-Bromohexyloxy)-9H-xanthen-9-one (**5d**). Synthesis as 2-(5-bromopentyloxy)-9*H*-xanthen-9-one from 2-hydroxyxanthone (**4a**) (10 mmol; 2.26 g) in NaOH solution (10 mmol; 0.4 g in 15 mL of water) with 1,6- dibromohexane (10 mmol; 2.44 g). Refluxed for 9 h. After cooling down the precipitate was filtered off, washed with water and ethanol. The crude product was used for the synthesis without further purification. White solid (2.6 g).

2-(6-Bromohexyloxy)-6-chloro-9H-xanthen-9-one (**5e**). Synthesis as 2-(5-bromopentyloxy)-9*H*-xanthen-9-one from 6-chloro-2-hydroxyxanthone (**4b**) (6 mmol; 1.48 g) in NaOH solution (6 mmol; 0.24 g in 10 mL of water) with 1,6- dibromohexane (6 mmol; 1.46 g). Refluxed for 5.5 h. After cooling down the precipitate was filtered off, washed with water and ethanol. The crude product was used for the synthesis without further purification. White solid (1 g).

2-(6-Bromohexyloxy)-7-chloro-9H-xanthen-9-one (**5f**). Synthesis as 2-(5-bromopentyloxy)-9*H*-xanthen-9-one from 6-chloro-2-hydroxyxanthone (**4c**) (6 mmol; 1.48 g) in NaOH solution (6 mmol; 0.24 g in 10 mL of water) with 1,6- dibromohexane (6 mmol; 1.46 g). Refluxed for 5.5 h. After cooling down the precipitate was filtered off, washed with water and ethanol. The crude product was used for the synthesis without further purification. White solid (1.4 g).

*4.1.2. General procedure for the synthesis of final compounds **6**–**28***

A proper bromoalkoxy-9H-xanthen-9-one (1 mmol) was added to the solution of a proper amine (2 mmol) in the mixture of ethanol (21 mL) and water (4 mL) in the presence of potassium carbonate (3 mmol) and KI (catalytic amount) and refluxed for 10–20 h. After cooling to RT the solid was filtered off. The filtrate was concentrated in vacuo and purified as described previously [33].

2-(5-(piperidin-1-yl*)pentyloxy)-9H-xanthen-9-one oxalate* (**6**). Synthesis from 2-(5-bromopentyloxy)-9*H*-xanthen-9-one (**5a**) (0.36 g, 1 mmol) and piperidine (0.17 g, 2 mmol). After purification was obtained 0.3 g of oil. Raw product was transformed into oxalic acid salt yielding 0.32 g (70%) of final compound. Mp: 167–169 °C. $C_{23}H_{27}NO_3$ x $C_2H_2O_4$ (MW = 455.49). ^{1}H NMR (400 MHz, DMSO-d_6) δ: 8.13–8.26 (m, 1H), 7.82–7.92 (m, 1H), 7.66 (t, J = 8.10 Hz, 2H), 7.56 (d, J = 2.7 Hz, 1H), 7.44–7.52 (m, 2H), 4.10 (t, J = 6.5 Hz, 2H), 2.84–3.27 (m, 6H), 1.64–1.92 (m, 8H), 1.40–1.63 (m, 4H). ^{13}C NMR (101 MHz, DMSO-d_6) δ: 176.24, 165.02, 155.98, 155.52, 150.68, 135.85, 126.40, 125.43, 124.68, 121.96, 120.95, 120.26, 118.65, 106.92, 68.30, 56.28, 52.48, 28.51, 23.45, 23.24, 23.06, 22.01. IR (cm^{-1}): 1652.10 (-C=O), 1210.62 (=C–O–C-), 1025.30 (=C–O–C-). LC-MS: purity 100% t_R = 5.17, (ESI) m/z $[M+H]^+$ 366.25. Anal. calcd. for $C_{25}H_{29}NO_7$: C, 65.92; H, 6.42; N, 3.07%. Found: C, 65.67; H, 6.56; N, 3.00%.

7-chloro-2-(5-(piperidin-1-yl*)pentyloxy)-9H-xanthen-9-one oxalate* (**7**). Synthesis from 2-(5-bromopentyloxy)-7-chloro-9H-xanthen-9-one (**5c**) (0.39 g, 0.001 mol) and piperidine (0.17 g, 0.002 mol). After purification was obtained 0.19 g of oil. Raw product was transformed into oxalic acid salt yielding 0.17 g (35%) of final compound. Mp: 198–200 °C. $C_{23}H_{26}NO_3Cl$ x $C_2H_2O_4$ (MW = 489.94). ^{1}H NMR (400 MHz, DMSO-d_6) δ: 8.11 (d, J = 2.2 Hz, 1H), 7.91 (dd, J = 2.2, 8.8 Hz, 1H), 7.74 (d, J = 8.8 Hz, 1H), 7.66 (d, J = 8.8 Hz, 1H), 7.43–7.59 (m, 2H), 4.00–4.21 (m, 2H), 2.85–3.23 (m, 5H), 1.60–1.93 (m, 9H), 1.49 (d, J = 6.6 Hz, 4H). ^{13}C NMR (101 MHz, DMSO-d_6) δ: 175.31, 164.89, 155.73, 154.56, 150.66, 135.60, 128.95, 125.85, 125.21, 121.99, 121.65, 121.22, 120.40, 106.83, 68.34, 56.32, 52.55, 28.49, 23.51, 23.22, 23.14, 22.03. LC-MS: purity 100% t_R = 5.95, (ESI) m/z $[M+H]^+$ 400.21. Anal. calcd. for $C_{25}H_{28}NO_7Cl$: C, 61.28; H, 5.76; N, 2.86%. Found: C, 61.53; H, 5.48; N, 2.83%.

2-(6-(piperidin-1-yl*)hexyloxy)-9H-xanthen-9-one oxalate* (**8**). Synthesis from 2-(6-bromohexyloxy)-9H-xanthen-9-one (**5d**) (0.38 g, 0.001 mol) and piperidine (0.17 g, 0.002 mol). After purification was obtained 0.15 g of oil. Raw product was transformed into oxalic acid salt yielding 0.18 g (38%) of final compound. Mp: 212–215 °C. $C_{24}H_{29}NO_3$ x $C_2H_2O_4$ (MW = 469.52). ^{1}H NMR (400 MHz, DMSO-d_6) δ: 8.21 (d, J = 7.0, 1.17 Hz, 1H), 7.79–7.96 (m, 1H), 7.39–7.74 (m, 5H), 4.11 (t, J = 6.10 Hz, 2H), 3.59–3.73 (m, 4H), 2.65–2.90 (m, 2H), 1.26–1.85 (m, 14H). ^{13}C NMR (101 MHz, DMSO-d_6) δ: 164.75, 159.85, 155.99, 155.57, 150.68, 135.88, 126.40, 125.47, 124.70, 121.98, 120.96, 120.29, 118.66, 106.87, 79.65, 72.71, 68.54, 58.54, 56.49, 53.20, 28.83, 26.58, 25.62, 19.03, 13.53. LC-MS: purity 99.06% t_R = 5.47, (ESI) m/z $[M+H]^+$ 380.27. Anal. calcd. for $C_{26}H_{31}NO_7$: C, 66.51; H, 6.65; N, 2.98%. Found: C, 66.70; H, 6.64; N, 2.94%.

6-Chloro-2-(6-(piperidin-1-yl*)hexyloxy)-9H-xanthen-9-one oxalate* (**9**). Synthesis from 2-(6-bromohexyloxy)-6-chloro-9H-xanthen-9-one (**5e**) (0.41 g, 0.001 mol) and piperidine (0.17 g, 0.002 mol). After purification was obtained 0.05 g of oil. Raw product was transformed into oxalic acid salt yielding 0.05 g (9%) of final compound. Mp: 213–216 °C. $C_{24}H_{28}NO_3Cl$ x $C_2H_2O_4$ (MW = 503.97). ^{1}H NMR (500 MHz, DMSO-d_6) δ: 8.15 (d, J = 8.59 Hz, 1H), 7.82 (d, J = 1.72 Hz, 1H), 7.60 (d, J = 9.16 Hz, 1H), 7.40–7.55 (m, 3H), 4.06 (t, J = 6.44 Hz, 2H), 3.04–3.26 (m, 3H), 2.73–3.02 (m, 3H), 1.54–1.82 (m, 8H), 1.16–1.50 (m, 6H). LC-MS: purity 93.01% t_R = 6.39, (ESI) m/z $[M+H]^+$ 414.17. Anal. calcd. for $C_{26}H_{30}NO_7Cl$: C, 61.96; H, 6.00; N, 2.78%. Found: C, 62.01; H, 5.78; N, 2.71%.

2-chloro-7-(6-(piperidin-1-yl*)hexyloxy)-9H-xanthen-9-one oxalate* (**10**). Synthesis from 2-(6-bromohexyloxy)-7-chloro-9H-xanthen-9-one (**5f**) (0.41 g, 0.001 mol) and piperidine (0.17 g, 0.002 mol). After purification was obtained 0.22 g of oil. Raw product was transformed into oxalic acid salt yielding 0.20 g (40%) of final compound. Mp: 190–193 °C. $C_{24}H_{28}NO_3Cl$ x $C_2H_2O_4$ (MW = 503.97). ^{1}H NMR (400 MHz, DMSO-d_6) δ: 8.12 (d, J = 2.20 Hz, 1H), 7.92 (dd, J = 2.42, 9.02 Hz, 1H), 7.75 (d, J = 8.80 Hz, 1H), 7.62–7.71 (m, 1H), 7.45–7.60 (m, 2H), 4.10 (t, J = 6.16 Hz, 2H), 3.89 (br s, 4H), 2.90–3.05 (m, 2H), 1.61–1.87 (m, 8H), 1.43–1.59 (m, 4H), 1.38 (d, J = 7.04 Hz, 2H). ^{13}C NMR (101 MHz, DMSO-d_6) δ: 175.33, 164.74, 155.77, 154.57, 150.65, 135.60, 128.95, 125.86, 125.22, 122.01, 121.66, 121.23, 120.40, 106.81, 68.55, 56.36, 52.53, 28.73, 26.29, 25.49, 23.73, 23.12, 21.97. LC-MS: purity 99.28% t_R = 6.35, (ESI) m/z $[M+H]^+$ 414.24. Anal. calcd. for $C_{26}H_{30}NO_7Cl$: C, 61.96; H, 6.00; N, 2.78%. Found: C, 61.98; H, 5.77; N, 2.66%.

2-(5-(3-methylpiperidin-1-yl*)pentyloxy)-9H-xanthen-9-one oxalate* (**11**). Synthesis from 2-(5-bromopentyloxy)-9*H*-xanthen-9-one (**5a**) (0.36 g, 0.001 mol) and 3-methylpiperidine (0.20 g, 0.002 mol). After purification was obtained 0.31 g of oil. Raw product was transformed into oxalic acid salt yielding 0.34 g (72%) of final compound. Mp: 156–158 °C. $C_{24}H_{29}NO_3$ x $C_2H_2O_4$ (MW = 469.52). ^{1}H NMR (400 MHz, DMSO-d_6) δ: 8.20 (dd, J = 1.17, 8.22 Hz, 1H), 7.83–7.92 (m, 1H), 7.65 (t, J = 8.41 Hz, 2H), 7.56 (d, J = 2.74 Hz, 1H), 7.42–7.52 (m, 2H), 4.10 (t, J = 6.26 Hz, 2H), 3.26–3.44 (m, 2H), 2.90–3.09 (m, 2H), 2.63–2.78 (m, 1H), 2.45 (t, J = 11.74 Hz, 1H), 1.61–1.98 (m, 8H), 1.39–1.56 (m, 2H), 0.98–1.15 (m, 1H), 0.89 (d, J = 6.65 Hz, 3H). ^{13}C NMR (101 MHz, DMSO-d_6) δ: 176.23, 165.05, 155.97, 155.51, 150.68, 135.84, 126.39, 125.43, 124.67, 120.26, 118.64, 106.92, 68.30, 57.91, 51.96, 30.58, 28.52, 23.45, 23.25, 19.06. IR (cm^{-1}): 1653.43 (-C=O), 1213.02 (=C–O–C-), 1025.45 (=C–O–C-). LC-MS: purity 100% t_R = 5.52, (ESI) m/z $[M+H]^+$ 380.21. Anal. calcd. for $C_{26}H_{31}NO_7$: C, 66.51; H, 6.65; N, 2.98%. Found: C, 66.03; H, 6.90; N, 2.91%.

6-chloro-2-(5-(3-methylpiperidin-1-yl*)pentyloxy)-9H-xanthen-9-one oxalate* (**12**). Synthesis from 2-(5-bromopentyloxy)-6-chloro-9H-xanthen-9-one (**5b**) (0.40 g, 0.001 mol) and 3-methylpiperidine (0.20 g, 0.002 mol). After purification was obtained 0.09 g of oil. Raw product was transformed into oxalic acid salt yielding 0.07 g (14%) of final compound. Mp: 138–141 °C. $C_{24}H_{28}NO_3Cl$ x $C_2H_2O_4$ (MW = 503.97). ^{1}H NMR (400 MHz, DMSO-d_6) δ: 8.17 (d, J = 8.6 Hz, 1H), 7.82 (d, J = 1.6 Hz, 1H), 7.61 (d, J = 9.0 Hz, 1H), 7.43–7.54 (m, 3H), 4.09 (t, J = 6.3 Hz, 2H), 3.25–3.45 (m, 2H), 2.92–3.07 (m, 2H), 2.72 (t, J = 11.3 Hz, 1H), 2.39–2.48 (m, 1H), 1.64–1.94 (m, 8H), 1.40–1.55 (m, 2H), 0.98–1.14 (m, 1H), 0.89 (d, J = 6.7 Hz, 3H). ^{13}C NMR (101 MHz, DMSO-d_6) δ: 175.54, 165.05, 156.23, 155.74, 150.58, 140.04, 128.28, 125.55, 125.22, 121.98, 120.24, 119.84, 118.49, 106.94, 68.33, 57.89, 51.95, 30.56, 28.51, 23.43, 23.24, 19.06. LC-MS: purity 100% t_R = 6.31, (ESI) m/z $[M+H]^+$ 414.17. Anal. calcd. for $C_{26}H_{30}NO_3Cl$: C, 61.96; H, 6.00; N, 2.78%. Found: C, 62.26; H, 5.83; N, 2.81%.

7-chloro-2-(5-(3-methylpiperidin-1-yl*)pentyloxy)-9H-xanthen-9-one oxalate* (**13**). Synthesis from 2-(5-bromopentyloxy)-7-chloro-9H-xanthen-9-one (**5c**) (0.39 g, 0.001 mol) and 3-methylpiperidine (0.20 g, 0.002 mol). After purification was obtained 0.24 g of oil. Raw product was transformed into oxalic acid salt yielding 0.22 g (44%) of final compound. Mp: 194–197 °C. $C_{24}H_{28}NO_3Cl$ x $C_2H_2O_4$ (MW = 503.97). ^{1}H NMR (400 MHz, DMSO-d_6) δ: 8.12 (d, J = 2.20 Hz, 1H), 7.91 (dd, J = 8.8, 2.6 Hz, 1H), 7.74 (d, J = 9.2 Hz, 1H), 7.67 (d, J = 8.8 Hz, 1H), 7.55 (d, J = 2.6 Hz, 1H), 7.51 (dd, J = 9.0, 2.9 Hz, 1H), 4.11 (t, J = 6.2 Hz, 2H), 3.24–3.43 (m, 2H), 2.89–3.07 (m, 2H), 2.70 (br s, 1H), 2.44 (br s, 1H), 1.58–1.94 (m, 8H), 1.39–1.56 (m, 2H), 0.97–1.13 (q, J = 11.89 Hz, 1H), 0.89 (d, J = 6.6 Hz, 3H). LC-MS: purity 99.07% t_R = 6.22, (ESI) m/z $[M+H]^+$ 414.24. Anal. calcd. for

$C_{26}H_{30}NO_7Cl$: C, 61.96; H, 6.00; N, 2.78%. Found: C, 62.03; H, 5.76; N, 2.73%.

2-(6-(3-Methylpiperidin-1-yl*)hexyloxy)-9H-xanthen-9-one oxalate* (**14**). Synthesis from 2-(6-bromohexyloxy)-9H-xanthen-9-one (**5d**) (0.38 g, 0.001 mol) and 3-methylpiperidine (0.20 g, 0.002 mol). After purification was obtained 0.28 g of oil. Raw product was transformed into oxalic acid salt yielding 0.28 g (58%) of final compound. Mp: 194–197 °C. $C_{25}H_{31}NO_3$ x $C_2H_2O_4$ (MW = 483.56). ^{1}H NMR (500 MHz, DMSO-d_6) δ: 8.16 (dd, J = 1.43, 8.02 Hz, 1H), 7.79–7.89 (m, 1H), 7.62 (t, J = 8.88 Hz, 2H), 7.52 (d, J = 3.15 Hz, 1H), 7.39–7.47 (m, 2H), 4.05 (t, J = 6.44 Hz, 2H), 3.21–3.36 (m, 2H), 2.92 (t, J = 7.59 Hz, 2H), 2.66 (t, J = 10.46 Hz, 1H), 2.41 (t, J = 11.46 Hz, 1H), 1.70–1.88 (m, 4H), 1.55–1.69 (m, 4H), 1.44 (qu, J = 7.52 Hz, 2H), 1.32 (qu, J = 7.30 Hz, 2H), 1.00 (q, J = 11.93 Hz, 1H), 0.84 (d, J = 6.59 Hz, 3H). ^{13}C NMR (126 MHz, DMSO-d_6) δ: 176.3, 165.1, 156.1, 155.6, 150.7, 136.0, 126.5, 125.5, 124.8, 122.0, 121.0, 120.4, 118.7, 106.9, 68.6, 58.0, 58.0, 57.9, 52.1, 30.6, 28.8, 26.4, 25.6, 23.7, 19.1. LC-MS: purity 100% t_R = 5.82, (ESI) m/z $[M+H]^+$ 394.30. Anal. calcd. for $C_{27}H_{33}NO_3$: C, 67.06; H, 6.88; N, 2.90%. Found: C, 67.40; H, 6.83; N, 2.89%.

6-chloro-2-(6-(3-methylpiperidin-1-yl*)hexyloxy)-9H-xanthen-9-one oxalate* (**15**). Synthesis from 2-(6-bromohexyloxy)-6-chloro-9H-xanthen-9-one (**5e**) (0.4 g, 0.001 mol) and 3-methylpiperidine (0.20 g, 0.002 mol). After purification was obtained 0.17 g of oil. Raw product was transformed into oxalic acid salt yielding 0.16 g (31%) of final compound. Mp: 193–196 °C. $C_{25}H_{30}NO_3Cl$ x $C_2H_2O_4$ (MW = 518.00). ^{1}H NMR (400 MHz, DMSO-d_6) δ: 8.08–8.25 (m, 1H), 7.86 (d, J = 1.76 Hz, 1H), 7.59–7.70 (m, 1H), 7.39–7.58 (m, 3H), 4.10 (t, J = 6.39 Hz, 2H), 3.22–3.42 (m, 2H), 2.97 (br s, 2H), 2.69 (d, J = 12.32 Hz, 1H), 2.35–2.48 (m, 1H), 1.58–1.88 (m, 7H), 1.43–1.55 (m, 2H), 1.31–1.41 (m, 2H), 1.17–1.28 (m, 1H), 0.99–1.08 (m, 1H), 0.89 (d, J = 6.17 Hz, 3H). IR (cm^{-1}): 1616.51 (-C=O), 1213.87 (=C–O–C-), 1073.96 (=C–O–C-). LC-MS: purity 95.19% t_R = 6.65, (ESI) m/z $[M+H]^+$ 428.19. Anal. calcd. for $C_{27}H_{32}NO_7Cl$: C, 62.60; H, 6.23; N, 2.70%. Found: C, 62.29; H, 5.96; N, 2.52%.

2-Chloro-7-(6-(3-methylpiperidin-1-yl*)hexyloxy)-9H-xanthen-9-one oxalate* (**16**). Synthesis from 2-(6-bromohexyloxy)-7-chloro-9H-xanthen-9-one (**5f**) (0.41 g, 0.001 mol) and 3-methylpiperidine (0.20 g, 0.002 mol). After purification was obtained 0.20 g of oil. Raw product was transformed into oxalic acid salt yielding 0.18 g (35%) of final compound. Mp: 164–166 °C. $C_{25}H_{30}NO_3Cl$ x $C_2H_2O_4$ (MW = 518.00). ^{1}H NMR (400 MHz, DMSO-d_6) δ: 8.09 (d, J = 2.3 Hz, 1H), 7.89 (dd, J = 2.7, 9.0 Hz, 1H), 7.72 (d, J = 9.0 Hz, 1H), 7.63 (d, J = 9.0 Hz, 1H), 7.42–7.55 (m, 2H), 4.08 (t, J = 6.5 Hz, 2H), 3.25–3.44 (m, 2H), 2.88–3.04 (t, 2H), 2.70 (t, J = 10.96 Hz, 1H), 2.44 (t, J = 11.7 Hz, 1H), 1.60–1.94 (m, 8H), 1.48 (qu, J = 7.3 Hz, 2H), 1.30–1.41 (qu, J = 7.04, Hz 2H), 1.05 (q, J = 12.27 Hz, 1H), 0.89 (d, J = 6.7 Hz, 3H). ^{13}C NMR (101 MHz, DMSO-d_6) δ: 175.3, 165.0, 155.7, 154.5, 150.6, 135.5, 128.9, 125.8, 125.2, 122.0, 121.6, 121.2, 120.3, 106.8, 68.5, 57.9, 52.0, 30.6, 28.7, 26.3, 25.5, 23.7, 19.1. IR (cm^{-1}): 1655.97 (-C=O), 1295.19 (=C–O–C-), 1022.74 (=C–O–C-). LC-MS: purity 99.33% t_R = 6.61, (ESI) m/z $[M+H]^+$ 428.38. Anal. calcd. for $C_{27}H_{32}NO_7Cl$: C, 62.60; H, 6.23; N, 2.70%. Found: C, 62.29; H, 6.13; N, 2.60%.

2-(5-(4-methylpiperidin-1-yl*)pentyloxy)-9H-xanthen-9-one oxalate* (**17**). Synthesis from 2-(5-bromopentyloxy)-9*H*-xanthen-9-one (**5a**) (0.36 g, 0.001 mol) and 4-methylpiperidine (0.20 g, 0.002 mol). After purification was obtained 0.28 g of oil. Raw product was transformed into oxalic acid salt yielding 0.27 g (58%) of final compound. Mp: 175–177 °C. $C_{24}H_{29}NO_3$ x $C_2H_2O_4$ (MW = 469.52). ^{1}H NMR (400 MHz, DMSO-d_6) δ: 8.20 (dd, J = 1.17, 7.83 Hz, 1H), 7.80–7.93 (m, 1H), 7.65 (t, J = 8.80 Hz, 2H), 7.55 (d, J = 3.13 Hz, 1H), 7.41–7.51 (m, 2H), 4.09 (t, J = 6.26 Hz, 2H), 3.37 (d, J = 11.35 Hz, 2H), 2.93–3.07 (m, 2H), 2.83 (t, J = 11.54 Hz, 2H), 1.66–1.87 (m, 6H), 1.60 (br s, 1H), 1.31–1.53 (m, 4H), 0.92 (d, J = 6.26 Hz, 3H). ^{13}C NMR (101 MHz, DMSO-d_6) δ: 176.2, 165.1, 156.0, 155.5, 150.7, 135.8, 126.4, 125.4, 124.7, 121.9, 120.9, 120.3, 118.6, 106.9, 68.3, 56.0, 51.9, 30.4, 28.5, 23.6, 23.3, 21.3. IR (cm^{-1}): 1658.68, (-C=O), 1214.77 (=C–O–C-), 1018.57 (=C–O–C-). LC-MS: purity 99.34% t_R = 5.50, (ESI) m/z $[M+H]^+$ 380.21. Anal. calcd. for $C_{26}H_{31}NO_7$: C, 66.51; H, 6.65; N, 2.98%. Found: C, 66.17; H, 6.92; N, 2.85%.

6-Chloro-2-(5-(4-methylpiperidin-1-yl*)pentyloxy)-9H-xanthen-9-one oxalate* (**18**). Synthesis from 2-(5-bromopentyloxy)-6-chloro-9H-xanthen-9-one (**5b**) (0.40 g, 0.001 mol) and 4-methylpiperidine (0.20 g, 0.002 mol). After purification was obtained 0.05 g of oil. Raw product was transformed into oxalic acid salt yielding 0.03 g (6%) of final compound. Mp: 168–171 °C. $C_{24}H_{28}NO_3Cl$ x $C_2H_2O_4$ (MW = 503.97). ^{1}H NMR (400 MHz, DMSO-d_6) δ: 8.19 (d, J = 8.61 Hz, 1H), 7.86 (d, J = 1.57 Hz, 1H), 7.64 (d, J = 9.00 Hz, 1H), 7.45–7.59 (m, 3H), 4.11 (t, J = 6.26 Hz, 2H), 3.37 (d, J = 10.96 Hz, 2H), 2.93–3.05 (m, 2H), 2.82 (br s, 2H), 1.66–1.87 (m, 6H), 1.60 (br s, 1H), 1.42–1.53 (m, 2H), 1.26–1.41 (m, 2H), 0.92 (d, J = 6.65 Hz, 3H). IR (cm^{-1}): 1656.54 (-C=O), 1214.03(=C–O–C-), 1074.77 (=C–O–C-). LC-MS: purity 100% t_R = 6.29, (ESI) m/z $[M+H]^+$ 414.17. Anal. calcd. for $C_{26}H_{30}NO_7Cl$: C, 61.96; H, 6.00; N, 2.78%. Found: C, 61.54; H, 5.86; N, 2.67%.

7-Chloro-2-(5-(4-methylpiperidin-1-yl*)pentyloxy)-9H-xanthen-9-one oxalate* (**19**). Synthesis from 2-(5-bromopentyloxy)-7-chloro-9H-xanthen-9-one (**5c**) (0.40 g, 0.001 mol) and 4-methylpiperidine (0.20 g, 0.002 mol). After purification was obtained 0.22 g of oil. Raw product was transformed into oxalic acid salt yielding 0.21 g (42%) of final compound. Mp: 205–208 °C. $C_{24}H_{28}NO_3Cl$ x $C_2H_2O_4$ (MW = 503.97). ^{1}H NMR (400 MHz, DMSO-d_6) δ: 8.13 (br s, 1H), 7.92 (d, J = 7.9 Hz, 1H), 7.63–7.81 (m, 2H), 7.41–7.62 (m, 2H), 4.12 (br s, 2H), 3.29–3.44 (m, 3H), 3.01 (br s, 2H), 2.84 (br s, 1H), 1.17–2.03 (m, 11H + H of solvent EtOH), 0.93 (d, J = 5.3 Hz, 3H). LC-MS: purity 98.24% t_R = 6.27, (ESI) m/z $[M+H]^+$ 414.24. Anal. calcd. for $C_{26}H_{30}NO_7Cl$: C, 61.96; H, 6.00; N, 2.78%. Found: C, 61.90; H, 5.75; N, 2.64%.

2-(6-(4-Methylpiperidin-1-yl*)hexyloxy)-9H-xanthen-9-one oxalate* (**20**). Synthesis from 2-(6-bromohexyloxy)-9H-xanthen-9-one (**5d**) (0.38 g, 0.001 mol) and 4-methylpiperidine (0.20 g, 0.002 mol). After purification was obtained 0.25 g of oil. Raw product was transformed into oxalic acid salt yielding 0.23 g (48%) of final compound. Mp: 186–189 °C. $C_{25}H_{31}NO_3$ x $C_2H_2O_4$ (MW = 483,54). ^{1}H NMR (500 MHz, DMSO-d_6) δ: 8.16 (dd, J = 1.1, 8.0 Hz, 1H), 7.90–7.78 (m, 1H), 7.62 (t, J = 8.6 Hz, 2H), 7.52 (d, J = 2.9 Hz, 1H), 7.41–7.47 (m, 2H), 4.05 (t, J = 6.3 Hz, 2H), 3.32 (d, J = 10.3 Hz, 2H), 2.86–2.98 (m, 2H), 2.78 (br s, 2H), 1.67–1.78 (m, 4H), 1.49–1.67 (m, 3H), 1.37–1.49 (m, 2H), 1.23–1.37 (m, 4H), 0.87 (d, J = 6.3 Hz, 3H). LC-MS: purity 98.95% t_R = 5.90, (ESI) m/z $[M+H]^+$ 394.23. Anal. calcd. for $C_{27}H_{33}NO_7$: C, 67.06; H, 6.88; N, 2.90%. Found: C, 67.35; H, 6.91; N, 2.86%.

6-Chloro-2-(6-(4-methylpiperidin-1-yl*)hexyloxy)-9H-xanthen-9-one oxalate* (**21**). Synthesis from 2-(6-bromohexyloxy)-6-chloro-9H-xanthen-9-one (**5e**) (0.41 g, 0.001 mol) and 4-methylpiperidine (0.20 g, 0.002 mol). After purification was obtained 0.16 g of oil. Raw product was transformed into oxalic acid salt yielding 0.16 g (31%) of final compound. Mp: 187–190 °C. $C_{25}H_{30}NO_3Cl$ x $C_2H_2O_4$ (MW = 518.00). ^{1}H NMR (400 MHz, DMSO-d_6) δ: 8.20 (d, J = 8.36 Hz, 1H), 7.86 (s, 1H), 7.60–7.73 (m, 1H), 7.40–7.58 (m, 3H), 4.03–4.17 (m, 2H), 3.26–3.47 (m, 3H), 2.99 (br s, 2H), 2.84 (br s, 1H), 1.72–1.85 (m, 4H), 1.67 (br s, 2H), 1.31–1.53 (m, 6H), 1.01–1.10 (m, 1H), 0.92 (d, J = 6.16 Hz, 3H). IR (cm^{-1}): 1609.59 (-C=O), 1215.36 (=C–O–C-), 1074.05 (=C–O–C-). LC-MS: purity 93.91% t_R = 6.65, (ESI) m/z $[M+H]^+$ 428.13. Anal. calcd. for $C_{27}H_{32}NO_3Cl$: C, 62.60; H, 6.23; N, 2.70%. Found: C, 62.37; H, 6.48; N, 2.74%.

2-Chloro-7-(6-(4-methylpiperidin-1-yl*)hexyloxy)-9H-xanthen-9-one oxalate* (**22**). Synthesis from 2-(6-bromohexyloxy)-7-chloro-9H-xanthen-9-one (**5f**) (0.41 g, 0.001 mol) and 4-methylpiperidine

(0.20 g, 0.002 mol). After purification was obtained 0.20 g of oil. Raw product was transformed into oxalic acid salt yielding 0.18 g (35%) of final compound. Mp: 182–185 °C. $C_{25}H_{30}NO_3Cl$ x $C_2H_2O_4$ (MW = 518.00). ^{1}H NMR (400 MHz, DMSO-d_6) δ: 8.11 (d, J = 2.7 Hz, 1H), 7.91 (dd, J = 2.7, 9.0 Hz, 1H), 7.74 (d, J = 9.0 Hz, 1H), 7.66 (d, J = 9.4 Hz, 1H), 7.45–7.58 (m, 2H), 4.10 (t, J = 6.25 Hz, 2H), 3.30–3.40 (m, 2H), 2.97 (t, J = 7.8 Hz, 2H), 2.65–2.85 (br s, 2H), 1.71–1.86 (m, 4H), 1.55–1.72 (m, 3H), 1.43–1.54 (m, 2H), 1.27–1.42 (m, 4H), 0.92 (d, J = 6.3 Hz, 3H). IR (cm^{-1}): 1666.59 (-C=O), 1295.97 (=C–O–C-), 1043.16 (=C–O–C-). LC-MS: purity 97.92% t_R = 6.64, (ESI) m/z $[M+H]^+$ 428.38. Anal. calcd. for $C_{27}H_{32}NO_7Cl$: C, 62.60; H, 6.23; N, 2.70%. Found: C, 62.21; H, 6.11; N, 2.51%.

2-(5-(Azepan-1-yl*)pentyloxy)-9H-xanthen-9-one oxalate* (**23**). Synthesis from 2-(5-bromopentyloxy)-9*H*-xanthen-9-one (**5a**) (0.36 g, 0.001 mol) and azepane (0.20 g, 0.002 mol). After purification was obtained 0.30 g of oil. Raw product was transformed into oxalic acid salt yielding 0.32 g (68%) of final compound. Mp: 140–142 °C. $C_{24}H_{29}NO_3$ x $C_2H_2O_4$ (MW = 469.52). ^{1}H NMR (400 MHz, DMSO-d_6) δ: 8.20 (dd, J = 7.83, 1.17 Hz, 1H), 7.84–7.91 (m, 1H), 7.65 (t, J = 8.80 Hz, 2H), 7.55 (d, J = 3.13 Hz, 1H), 7.44–7.51 (m, 2H), 4.09 (t, J = 6.26 Hz, 2H), 3.37 (d, J = 11.35 Hz, 2H), 2.95–3.03 (m, 2H), 2.83 (m, J = 11.54 Hz, 2H), 1.67–1.84 (m, 6H), 1.60 (br s, 1H), 1.32–1.53 (m, 4H), 0.92 (d, J = 6.26 Hz, 3H). ^{13}C NMR (101 MHz, DMSO-d_6) δ: 176.24, 165.13, 155.98, 155.52, 150.68, 135.84, 126.39, 125.43, 124.67, 121.96, 120.95, 120.26, 118.64, 106.92, 68.33, 56.65, 54.00, 28.53, 26.53, 23.88, 23.54, 23.24. IR (cm^{-1}): 1652.51 (-C=O), 1212,53 (=C–O–C-), 1027.28 (=C–O–C-). LC-MS: purity 100% t_R = 5.42, (ESI) m/z $[M+H]^+$ 380.21. Anal. calcd. for $C_{26}H_{31}NO_7$: C, 66.51; H, 6.65; N, 2.98%. Found: C, 66.42; H, 6.88; N, 2.87%.

2-(5-(Azepan-1-yl*)pentyloxy)-6-chloro-9H-xanthen-9-one oxalate* (**24**). Synthesis from 2-(5-bromopentyloxy)-6-chloro-9H-xanthen-9-one (**5b**) (0.36 g, 0.001 mol) and azepane (0.20 g, 0.002 mol). After purification was obtained 0.16 g of oil. Raw product was transformed into oxalic acid salt yielding 0.16 g (32%) of final compound. Mp: 139–141 °C. $C_{24}H_{28}NO_3Cl$ x $C_2H_2O_4$ (MW = 503.97). ^{1}H NMR (400 MHz, DMSO-d_6) δ 8.15 (d, J = 8.61 Hz, 1H), 7.80 (d, J = 1.96 Hz, 1H), 7.59 (d, J = 9.00 Hz, 1H), 7.54–7.42 (m, 3H), 4.08 (t, J = 6.26 Hz, 2H), 3.31–3.14 (m, 4H), 3.12–2.98 (m, 2H), 1.89–1.68 (m, 8H), 1.60 (br s, 4H), 1.54–1.39 (m, 2H). ^{13}C NMR (101 MHz, DMSO-d_6) δ: 176.24, 165.13, 155.98, 155.52, 150.68, 135.84, 126.39, 125.43, 124.67, 121.96, 120.95, 120.26, 118.64, 106.92, 68.33, 56.65, 54.00, 28.53, 26.53, 23.88, 23.54, 23.24. IR (cm^{-1}): 1656.96 (-C=O), 1616.48, 1213.44 (=C–O–C-), 1074.49 (=C–O–C-). LC-MS: purity 100% t_R = 6.21, (ESI) m/z $[M+H]^+$ 414.17. Anal. calcd. for $C_{26}H_{30}NO_7Cl$: C, 61.96; H, 6.00; N, 2.78%. Found: C, 61.62; H, 5.85; N, 2.65%.

2-(5-(Azepan-1-yl*)pentyloxy)-7-chloro-9H-xanthen-9-one oxalate* (**25**). Synthesis from 2-(5-bromopentyloxy)-7-chloro-9H-xanthen-9-one (**5c**) (0.40 g, 0.001 mol) and azepane (0.20 g, 0.002 mol). After purification was obtained 0.22 g of oil. Raw product was transformed into oxalic acid salt yielding 0.21 g (42%) of final compound. Mp: 183–186 °C. $C_{24}H_{28}NO_3Cl$ x $C_2H_2O_4$ (MW = 503.97). ^{1}H NMR (400 MHz, DMSO-d_6) δ: 8.05 (d, J = 2.35 Hz, 1H), 7.87 (dd, J = 9.00, 2.74 Hz, 1H), 7.69 (d, J = 9.00 Hz, 1H), 7.60 (d, J = 8.61 Hz, 1H), 7.43–7.54 (m, 2H), 4.07 (t, J = 6.26 Hz, 2H), 3.15–3.31 (m, 4H), 2.97–3.12 (m, 2H), 1.89 (m, 8H), 1.60 (br s, 4H), 1.47 (qu, J = 7.34 Hz, 2H). ^{13}C NMR (101 MHz, DMSO-d_6) δ: 175.19, 165.23, 155.67, 154.47, 150.56, 135.49, 128.89, 125.75, 125.15, 121.90, 121.55, 121.13, 120.29, 106.76, 68.36, 56.62, 53.94, 28.52, 26.55, 23.83, 23.46, 23.25LC-MS: purity 100% t_R = 6.16, (ESI) m/z $[M+H]^+$ 414.25. Anal. calcd. for $C_{26}H_{30}NO_7Cl$: C, 61.96; H, 6.00; N, 2.78%. Found: C, 62.08; H, 5.79; N, 2.74%.

2-(6-(Azepan-1-yl*)hexyloxy)-9H-xanthen-9-one oxalate* (**26**). Synthesis from 2-(6-bromohexyloxy)-9H-xanthen-9-one (**5d**) (0.38 g, 0.001 mol) and azepane (0.20 g, 0.002 mol). After purification was obtained 0.26 g of oil. Raw product was transformed into oxalic acid salt yielding 0.20 g (42%) of final compound. Mp: 180–182 °C. $C_{25}H_{31}NO_3$ x $C_2H_2O_4$ (MW = 483.54). ^{1}H NMR (400 MHz, DMSO-d_6) δ: 8.20 (dd, J = 1.17, 8.22 Hz, 1H), 7.81–7.93 (m, 1H), 7.65 (t, J = 8.41 Hz, 2H), 7.55 (d, J = 2.74 Hz, 1H), 7.42–7.51 (m, 2H), 4.09 (t, J = 6.26 Hz, 2H), 3.20 (br s, 4H), 2.95–3.08 (m, 2H), 1.54–1.89 (m, 12H), 1.43–1.53 (m, 2H), 1.31–1.41 (m, 2H). ^{13}C NMR (101 MHz, DMSO-d_6) δ: 176.24, 165.10, 155.98, 155.55, 150.66, 135.84, 126.39, 125.44, 124.67, 121.96, 120.95, 120.26, 118.64, 106.87, 68.49, 56.70, 53.98, 28.76, 26.31, 23.52. IR (cm^{-1}): 1654.09 (-C=O), 1626.78, 1216.75 (=C–O–C-), 1025.42 (=C–O–C-). LC-MS: purity 97.44% t_R = 5.77, (ESI) m/z $[M+H]^+$ 394.23. Anal. calcd. for $C_{27}H_{33}NO_7$: C, 67.06; H, 6.88; N, 2.90%. Found: C, 66.91; H, 6.70; N, 2.75%.

2-(6-(azepan-1-yl*)hexyloxy)-6-chloro-9H-xanthen-9-one oxalate* (**27**). Synthesis from 2-(6-bromohexyloxy)-6-chloro-9H-xanthen-9-one (**5e**) (0.41 g, 0.001 mol) and azepane (0.20 g, 0.002 mol). After purification was obtained 0.09 g of oil. Raw product was transformed into oxalic acid salt yielding 0.07 g (14%) of final compound. Mp: 190–193 °C. $C_{25}H_{30}NO_3Cl$ x $C_2H_2O_4$ (MW = 518.00). ^{1}H NMR (400 MHz, DMSO-d_6) δ: 8.19 (d, J = 8.61 Hz, 1H), 7.85 (d, J = 1.56 Hz, 1H), 7.64 (d, J = 9.00 Hz, 1H), 7.46–7.58 (m, 3H), 4.08–4.13 (m, 2H), 3.19–3.35 (m, 3H), 2.95–3.18 (m, 3H), 1.79 (br s, 6H), 1.56–1.70 (m, 6H), 1.44–1.52 (m, 2H), 1.33–1.42 (m, 2H). ^{13}C NMR (101 MHz, DMSO-d_6) δ 175.6, 164.8, 156.3, 155.8, 150.6, 140.1, 128.3, 125.6, 125.3, 122.0, 120.3, 119.9, 118.5, 107.0, 68.6, 56.7, 54.1, 28.7, 26.4, 26.3, 25.5, 24.0, 23.5. IR (cm^{-1}): 1614.41 (-C=O), 1214.76 (=C–O–C-), 1074.28 (=C–O–C-). LC-MS: purity 94.98% t_R = 6.57, (ESI) m/z $[M+H]^+$ 428.19. Anal. calcd. for $C_{27}H_{32}NO_7Cl$: C, 62.60; H, 6.23; N, 2.70%. Found: C, 62.23; H, 6.25; N, 2.53%.

2-(6-(Azepan-1-yl*)hexyloxy)-7-chloro-9H-xanthen-9-one oxalate* (**28**). Synthesis from 2-(6-bromohexyloxy)-7-chloro-9H-xanthen-9-one (**5f**) (0.41 g, 0.001 mol) and azepane (0.20 g, 0.002 mol). After purification was obtained 0.20 g of oil. Raw product was transformed into oxalic acid salt yielding 0.16 g (31%) of final compound. Mp: 172–175 °C. $C_{25}H_{30}NO_3Cl$ x $C_2H_2O_4$ (MW = 518.00). ^{1}H NMR (400 MHz, DMSO-d_6) δ: 8.08 (d, J = 2.3 Hz, 1H), 7.89 (dd, J = 2.3, 9.0 Hz, 1H), 7.71 (d, J = 9.0 Hz, 1H), 7.62 (d, J = 9.0 Hz, 1H), 7.39–7.55 (m, 2H), 4.07 (t, J = 6.3 Hz, 2H), 3.20 (br. s. 4H), 2.93–3.09 (m, 2H), 1.78 (m, 6H), 1.64–1.73 (m, 2H), 1.60 (m, 4H), 1.42–1.53 (qu, 2H), 1.29–1.42 (def qu, 2H). ^{13}C NMR (101 MHz, DMSO-d_6) δ: 175.24, 165.13, 155.73, 154.51, 150.58, 135.53, 128.90, 125.79, 125.18, 121.60, 121.16, 120.33, 106.75, 68.53, 56.69, 53.96, 28.75, 26.52, 23.48. IR (cm^{-1}): 1665.94 (-C=O), 1295.11(=C–O–C-), 1022.80 (=C–O–C-). LC-MS: purity 99.68% t_R = 6.59, (ESI) m/z $[M+H]^+$ 428.38. Anal. calcd. for $C_{25}H_{30}NO_3Cl$ x $C_2H_2O_4$: C, 62.60; H, 6.23; N, 2.70%. Found: C, 62.32; H, 6.20; N, 2.60%.

4.2. In vitro biological studies

4.2.1. Radioligand binding assay to histamine H_3 receptor

Affinity to human histamine H_3 receptor was evaluated in a radioligand binding assay with N^{α}-methylhistamine as a radioligand in CHO K1 cells as described by Łażewska et al. [44]. Ten mM stock solutions of tested compounds were prepared in DMSO. Serial dilutions of compounds were prepared in 96-well microplate in assay buffers using automated pipetting system epMotion 5070 (Eppendorf). Each compound was tested in 6 concentrations from 10^{-5} to 10^{-10} M (final concentration). All assays were carried out in duplicate. Radioactivity was counted in MicroBeta2 scintillation counter (PerkinElmer). Data were fitted to a one-site curve-fitting equation with GraphPad Prism 6 (GraphPad Software, San Diego, CA, USA) and K_i values were estimated from the Cheng–Prusoff equation [64].

4.2.2. Inhibition of cholinesterases

Inhibitory activities of the tested compounds against cholinesterases were measured using a spectrophotometric method as described by Ellman et al. [36] with small modifications [16].

Firstly, compounds were tested at a screening concentration of 10 μM. To determine IC_{50} value, the absorbance measured at six different concentrations of inhibitor was converted to % inhibition of enzyme and plotted against the applied inhibitor concentration, using nonlinear regression with GraphPad Prism 5 (GraphPad Software, San Diego, CA, USA). Donepezil and tacrine were used as the reference compounds. All assays were performed in triplicate.

4.2.3. Kinetic studies of eeAChE and eqBuChE inhibition

The kinetic studies were performed with compounds **23** and **25**, using Ellman's method [36], modified for 96-well microplates [16]. Inhibitors were tested in the concentrations giving enzyme activities between 30% and 80%. For each concentration of the inhibitor, substrate (ATC/BTC) was added at concentrations of 0.3, 0.24, 0.18, 0.12, 0.06, and 0.04 mM in the wells. Each experiment was performed in triplicate. V_{max} and K_m values of the Michaelis–Menten kinetics were calculated by nonlinear regression from substrate–velocity curves. Lineweaver-Burk and Cornish-Bowden plots were calculated using linear regression in GraphPad Prism 5 (GraphPad Software, San Diego, CA, USA).

4.2.4. Inhibition of monoamine oxidase A and B

Inhibition of MAO isoenzymes was evaluated by a fluorometric method using Amplex Red Monoamine Oxidase kits (ThermoFisher Scientific A12214, Waltham, MA, USA) as described by Łażewska et al. [44]. For all tests recombinant human MAO B and MAO A (from Sigma AldrichM7441 and M7316, Darmstadt, Germany) were used. Inhibitory activity of compounds was measured in the presence of p-tyramine (200 μM). As references were used for MAO-B: pargyline 10 μM, rasagiline 1 μM, safinamide 1 μM, and for MAO-A clorgyline 1 μM. For *h*MAO B inhibitory activity compounds were tested in a concentration of 1 μM. Then, IC_{50} were obtained from concentration–response curves. All calculations were made in Microsoft Excel and GraphPad Prism 5 (GraphPad Software, San Diego, CA, USA). All experiments were performed in duplicate, and data are expressed as mean ± SEM of 2–5 independent experiments. For *h*MAO A inhibition compounds were tested first at a concentration of 10 μM, and then at a concentration of 1 μM. None of compounds showed in these screenings inhibition higher that 50%. Thus, no further studies were performed.

4.3. Molecular modeling

4.3.1. Molecular docking to histamine H_3 receptor

For docking purposes, Schrödinger Maestro Suite (v. 11.5.011, Release 2018–01) was used [65]. Ligands were built in their ionized forms (protonated N1 piperidine nitrogen atom, structure charge +1) and their bioactive conformations were generated using ConfGen module [66,67] (water environment, target number of conformers − 20). Binding site was centered on ligand placed in homology model (pitolisant). Docking to rigid form of receptor was performed using Glide module [68–70] (extra precision, flexible ligand sampling, max 5 poses per conformer). Ligands were rated according their position in binding pocket, interactions with binding pocket amino acids, as well as the docking score value. Ligand interaction diagrams were generated using Schrödinger Maestro, ligand-receptor visualizations were generated using UCSF Chimera [71].

4.3.2. Molecular docking to acetylcholinesterase, butyrylcholinesterase and monoamine oxidase B

Docking studies were performed according to the previously validated procedures [42,44]. The tested compounds were prepared in Corina online. Next, bond and atom types were checked. Charges and hydrogen atoms were added in Sybyl 8.0 (Tripos). Ligands were docked into the active site of enzymes: acetylcholinesterase (PDB code: 1EVE), butyrylcholinesterase (PDB code: 1P0I) and human monoamine oxidase B (PDB code: 4A79). Before docking, crystal structures of enzymes were downloaded from Protein Data Bank and prepared as follow: the hydrogen atoms were added, all histidine were protonated at Nε atoms. Ligand and water molecules were removed, except water molecules 1159, 1249 and 1254 in AChE. Binding sites were defined within the radius of 10 Å, 20 Å and 12 Å from the reference ligands – donepezil, butyrate and pioglitazone for AChE, BuChE and hMAO B, respectively. Docking studies were performed twice for each enzyme in GOLD 5.1 software. Standard parameters of genetic algorithm with population size 100 and operation number 100,000 were applied. For each ligand 2 × 10 poses were generated and sorted according to the ChemScore value. Binding modes were analyzed in PyMOL software.

4.4. In vivo pharmacological studies

4.4.1. Analgesic effect of selected compounds

4.4.1.1. Animals. The experiments were carried out on adult male Albino Swiss mice (CD-1, 18–25 g) and male Wistar rats (Krf:(WI) WU), 180–250 g) obtained from the Animal House of the Faculty of Pharmacy, Jagiellonian University Medical College. Animals were housed in plastic cages in room at a constant temperature of 20 ± 2 °C, under light/dark (12:12) cycle and had free access to standard pellet diet and water. Experimental protocols were proved by the Local Ethics Committee on Animal Experimentation in Kraków, Poland (Resolution No: 139/2017 and 179/2017). All animal procedures were in accordance with the European Union Directive (2010/63/EU) and the Polish regulations.

4.4.1.2. Formalin test in mice. The procedure used was essentially the same as that described previously [46,47]. Briefly, the pain was induced by the intraplantar injection of 20 μL of 2.5% formalin solution into the mice right hind paw. The total time (in s) spent on licking the injected paw during periods of 0–5 min (early phase, neurogenic) and 15–30 min (late phase, inflammatory) was measured and was considered as an indicator of nociceptive behaviour. Before formalin injection mice were treated i.p. with: vehicle (10 mL/kg, negative control) or investigated compounds at the doses of 15, 22.5 and 30 mg/kg.

4.4.1.3. Carageenan-induced paw oedema, mechanical and thermal hypernociception in rats. The acute, local inflammation and paw oedema was induced by subplantar injection of 0.1 mL of 1% carrageenan (made in PBS) into the rat right hind paw. The paw volume was measured by the dislocation of the water column of the plethysmometer (Plethysmometr 7140, Ugo Basile). The pain pressure threshold was used to measure the hyperalgesic response to mechanical stimuli. Increasing pressure was applied to the dorsal surface of the right hind paw by an automated gauge (Analgesy Meter 37215, Ugo Basile) according to the method of Randall and Selitto. The intensity of the applied force, in grams, was recorded when the paw was withdrawn (withdrawal threshold). The hyperalgesic response to thermal stimuli was determined by using a plantar test apparatus (Commat Ltd. Turkey). Rats were placed individually in plexiglas chambers and allowed to acclimatize for 20–30 min before testing. The radiant heat was positioned under

the chamber floor directly beneath the hind paw and the latency to paw withdrawal was automatically recorded by a photocell and an electronic timer [48].

4.4.1.4. Oxaliplatin-induced neuropathic pain in mice. Neuropathy was induced by the administration of a single dose (10 mg/kg) of Oxaliplatin (OXPT) dissolved in a 5% glucose solution (Polfa Kutno, Poland). To assess the sensitivity to mechanical stimuli the von Frey test was carried out using the electronic von Frey unit (Bioseb, France). The apparatus was supplied with a single flexible filament, which was used to apply increasing force (from 0 to 10 g) against the plantar surface of the hind paw of the mouse. The crossing of pain threshold resulted in the paw withdrawal and subsequent recording of the mechanical pressure that evoked the nocifensive response. The measurement was done before the OXPT administration, 3 h and 7 days afterwards. The compounds were administrated to the animals with tactile allodynia observed as a statistically significant decrease in pain threshold. On the day of the experiment, each mouse was placed in an observation chamber with a wire mesh bottom and was allowed to habituate for 1 h. After the habituation period, the mouse pain threshold was tested 3 times alternately with at least 30 s gap between each measurement. The mean of these three consecutive measurements was taken as a baseline value. The mice with tactile allodynia were i.p. pretreated with the tested compound and 30 min later the animals were tested again according to the same procedure [72].

*4.4.2. Memory-enhancing effects of test compounds **23** and **25***

4.4.2.1. Animals. Inbred male Wistar rats were used in the current study to assess memory-enhancing effects of test compounds **23** and **25**. The rats were obtained from the central animal facility in UAE University. The animals were kept in a specific room with controlled temperature and humidity (24 °C ± 2 °C and 55% ± 15%, respectively), 12/12-h light/dark sequence, and free access to food and water. All the rats were 6–8 weeks of age and weighed 189–230 g. The behavioural experiments assessing memory were performed each day between 09:00 a.m. and 01:00 p.m. by the same investigator in a blinded manner; all procedures were performed in accordance with the guidelines of the European Communities Council Directive of November 24, 1986 (86/609/EEC) and approval was obtained from the Institutional Animal Ethics Committee in College of Medicine and Health Sciences/United Arab Emirates University (A30-13) before the experiments were started. All efforts were made to minimize the total number of the animals used and their pain.

4.4.2.2. Step-through inhibitory avoidance paradigm (SIAP). Memory deficit was assessed by step through inhibitory avoidance apparatus (Step-through Cage, 7550; Ugo Basile, Comerio, Italy), as described previously [15,52–58]. The experiment consists of two trials (training and testing), in the training day each rat was placed in the white compartment and after 30 s habituation time the door was raised automatically and once the rat with all his four paws entered the dark compartment the door was closed and a foot shock of 0.4 mA (20 Hz, 8.3 ms) was delivered to the grid floor for 3 s, and step-through latency (STL) time was measured. Immediately after the foot shock rats were returned to its home cage. Rats that had step through latency more than 60 s were excluded from the experiment. 24 h later, in the test day STL time was measured in the same way with no foot shock, however the cut off-time was increased to 300 s. The reduction of STL time was used as an indicator for memory impairment.

4.4.2.3. Transfer latency paradigm time (TLPT) in elevated plus maze test. During the acquisition trial in the first day (training day) each rat was placed at the distal ending of one of the open arms facing away from central platform. Transfer latency time (TLT), the time required for the rat to enter any of the closed arms with its four paws, was measured with a cut off-time at 80s. After the animal entered the closed arm by 10 s the rat was returned to its home cage. Memory retention was examined 24 h later (test day), applying the same protocol of the first day, however, evaluating different test groups (as explained for SIAP) administered with DIZ (0.1 mg/kg, i.p.), different doses of **23** (1.25, 2.5, and 5 mg/kg, i.p.), different doses of **25** (1.25, 2.5, and 5 mg/kg, i.p.), or reference drug donepezil (DOZ, 1 mg/kg, i.p.). Prolonged retention of transfer latency time (TLT) was considered as an indicator of impaired memory as previously described [54,57,73,74].

The data were analyzed for normality through assessment of the sample distribution or skewness where −1.3 to +1.3 was considered to be normally distributed. After the results had passed the tests for normality, they were analyzed where applicable using one- or two-way ANOVA followed by Tukey's post hoc test. For statistical comparisons, the software package SPSS 25.0 (IBM Middle East, Dubai, UAE) was used. The results are expressed as the mean and standard error of the mean (SEM). *P*-values, 0.05 were considered to indicate statistical significance.

4.5. Permeability

The PAMPA Plate System Gentest™ was used for estimation of compounds passive penetration through cell membranes and was provided by Corning (Tewksbury, MA, USA). The assay was performed in accordance to the manufacturer recommendations and was previously described by our research group [61]. Briefly, 10 mM stocks (DMSO) of tested compounds were diluted to 200 μM in PBS (phosphate-buffered saline, pH 7.4) and added to the donor wells. Wells on the receiver plate were filled only with PBS. After 5 h of incubation at the room temperature the concentrations of tested compounds in wells were estimated using the LC/MS method with an internal standard. Mass spectra (LC/MS) were performed on API 3200 mass spectrometer (Sciex, Framingham, MA, USA) coupled to HPLC Shimadzu LC-20AT (Shimadzu, Duisburg, Germany). The assay was performed in triplicate. The permeability coefficient P_e was calculated according to the formulas described in the literature [62,75] and compared to the high permeable reference caffeine.

Declaration of competing interest

The authors declare that they have no known competing financial interests or personal relationships that could have appeared to influence the work reported in this paper.

Acknowledgments

This research was funded by National Science Centre, Poland grant: No UMO-2016/23/B/NZ7/02327 (DŁ) (synthesis and *in vitro* studies). *In vivo* analgesic studies were financially supported by Jagiellonian University Medical College grant no. N42/DBS/000047 (SM). Support for *in vivo* procognitive studies was provided to BS by College of Medicine and Health Sciences and the Office of Graduate Studies and Research, United Arab Emirates University (UAEU Program for Advanced Research, grant number#31M310). Further, the authors (DŁ, KK-K) acknowledge the contribution of EU-COST action CA18133 ("European Research Network on Signal Transduction").

Appendix A. Supplementary data

Supplementary data to this article can be found online at

https://doi.org/10.1016/j.ejmech.2020.112743.

References

[1] M. Batool, B. Ahmad, S. Choi, A structure-based drug discovery paradigm, Int. J. Mol. Sci. 20 (2019) 2783, https://doi.org/10.3390/ijms20112783.

[2] T. Cheng, Q. Li, Z. Zhou, Y. Wang, S.H. Bryant, Structure-based virtual screening for drug discovery: a problem-centric review, AAPS J. 14 (2012) 133–141, https://doi.org/10.1208/s12248-012-9322-0.

[3] E.J. Proschak, H. Stark, D. Merk, Polypharmacology by design: a medicinal chemist's perspective on multitargeting compounds, J. Med. Chem. 62 (2019) 420–444, https://doi.org/10.1021/acs.jmedchem.8b00760.

[4] C.A. Lane, J. Hardy, J.M. Schott, Alzheimer's disease, Eur. J. Neurol. 25 (2018) 59–70, https://doi.org/10.1111/ene.13439.

[5] R. Adolfsson, C.-G. Gottfries, L. Oreland, Å. Wiberg, B. Winblad, Increased activity of brain and platelet monoamine oxidase in dementia of Alzheimer type, Life Sci. 27 (1980) 1029–1034, https://doi.org/10.1016/0024-3205(80)90025-9.

[6] S. Schedin-Weiss, M. Inoue, L. Hromadkova, Y. Teranishi, N.G. Yamamoto, B. Wiehager, N. Bogdanovic, B. Winblad, A. Sandebring-Matton, S. Frykman, L.O. Tjernberg, Monoamine oxidase B is elevated in Alzheimer disease neurons, is associated with γ-secretase and regulates neuronal amyloid β-peptide levels, Alzheimer's Res. Ther. 9 (2017) 57, https://doi.org/10.1186/s13195-017-0279-1.

[7] B.S. Husebo, W. Achterberg, E. Flo, Identifying and managing pain in people with Alzheimer's disease and other types of dementia: a systematic review, CNS Drugs 30 (2016) 481–497, https://doi.org/10.1007/s40263-016-0342-7.

[8] S. Cao, D.W. Fisher, T. Yu, H. Dong, The link between chronic pain and Alzheimer's disease, J. Neuroinflammation 16 (2019) 204, https://doi.org/10.1186/s12974-019-1608-z.

[9] P. Panula, P.L. Chazot, M. Cowart, R. Gutzmer, R. Leurs, W.L. Liu, H. Stark, R.L. Thurmond, H.L. Haas, International union of basic and clinical pharmacology. XCVIII. Histamine receptors, Pharmacol. Rev. 67 (2015) 601–655, https://doi.org/10.1124/pr.114.010249.

[10] B. Sadek, D. Łażewska, S. Hagenow, K. Kieć-Kononowicz, H. Stark, Histamine H_3R antagonists: from scaffold hopping to clinical candidates, in: P. Blandina, M.B. Passani (Eds.), Histamine Receptors, Springer International Publishing Cham, Switzerland, 2016, pp. 109–156.

[11] I. Obara, V. Telezhkin, I. Alrashdi, P.L. Chazot Histamine, Histamine receptors, and neuropathic pain relief, Br. J. Pharmacol. 177 (2020) 580–599, https://doi.org/10.1111/bph.14696.

[12] N. Ghamari, O. Zarei, J.A. Arias-Montaño, D. Reiner, S. Dastmalchi, H. Stark, M. Hamzeh-Mivehroud, Histamine H_3 receptor antagonists/inverse agonists: where do they go? Pharmacol. Ther. 200 (2019) 69–84, https://doi.org/10.1016/j.pharmthera.2019.04.007.

[13] D. Łażewska, K. Kieć-Kononowicz, Progress in the development of histamine H_3 receptor antagonists/inverse agonists: a patent review (2013–2017), Expert Opin. Ther. Pat. 28 (2018) 175–196, https://doi.org/10.1080/13543776.2018.1424135.

[14] F.H. Darras, S. Pockes, G. Huang, A. Strasser, H.-J. Wittman, M. Nimczick, C.A. Sotriffer, M. Decker, Synthesis, biological evaluation, and computational studies of tri- and tetracyclic nitrogen-bridgehead compounds as potent dual-acting AChE inhibitors and hH$_3$ receptor antagonists, ACS Chem. Neurosci. 5 (2014) 225–242, https://doi.org/10.1021/cn4002126.

[15] N. Khan, A. Saad, S.M. Nurulain, F.H. Darras, M. Decker, B. Sadek, The dual-acting H_3 receptor antagonist and AChE inhibitor UW-MD-71 dose-dependently enhances memory retrieval and reverses dizocilpine-induced memory impairment in rats, Behav. Brain Res. 297 (2016) 155–164, https://doi.org/10.1016/j.bbr.2015.10.022.

[16] M. Bajda, D. Łażewska, J. Godyń, P. Zaręba, K. Kuder, S. Hagenow, K. Łątka, E. Stawarska, H. Stark, K. Kieć-Kononowicz, K. Malawska, B. Search for new multi-target compounds against Alzheimer's disease among histamine H_3 receptor ligands, Eur. J. Med. Chem. 185 (2020) 111785, https://doi.org/10.1016/j.ejmech.2019.111785.

[17] Ó.M. Bautista-Aguilera, S. Hagenow, A. Palomino-Antolin, V. Farré-Alins, L. Ismaili, P.L. Joffrin, M.L. Jimeno, O. Soukup, J. Janočková, L. Kalinowsky, E. Proschak, I. Iriepa, I. Moraleda, J.S. Schwed, A. Romero Martínez, F. López-Muñoz, M. Chioua, J. Egea, R.R. Ramsay, J. Marco-Contelles, H. Stark, Multi-target-directed ligands combining cholinesterase and monoamine oxidase inhibition with histamine H_3R antagonism for neurodegenerative diseases, Angew. Chem., Int. Ed. Engl. 56 (2017) 12765–12769, https://doi.org/10.1002/anie.201706072.

[18] Ó.M. Bautista-Aguilera, J. Budni, F. Mina, E.B. Medeiros, W. Deuther-Conrad, J.M. Entrena, I. Moraleda, I. Iriepa, F. López-Muñoz, J. Marco-Contelles, Contilisant, a tetratarget small molecule for Alzheimer's disease therapy combining cholinesterase, monoamine oxidase inhibition, and H_3R antagonism with S_1R agonism profile, J. Med. Chem. 61 (2018) 6937–6943, https://doi.org/10.1021/acs.jmedchem.8b00848.

[19] S. Irshad Ahmad, Recent insight into the biological activities of synthetic xanthone derivatives, Eur. J. Med. Chem. 116 (2016) 267–280, https://doi.org/10.1016/j.ejmech.2016.03.058.

[20] L.C. Klein-Júnior, A. Campos, R. Niero, R. Corrêa, Y. Vander Heyden, V.C. Filho, Xanthones and cancer: from natural sources to mechanisms of action, Chem. Biodivers. 17 (2019), e1900499, https://doi.org/10.1002/cbdv.201900499.

[21] D.R.P. Loureiro, J.X. Soares, J.C. Costa, Á.F. Magalhães, C.M.G. Azevedo, M.M.M. Pinto, C.M.M. Afonso, Structures, activities and drug-likeness of anti-infective xanthone derivatives isolated from the marine environment: a review, Molecules 24 (2019) e243, https://doi.org/10.3390/molecules24020243.

[22] C.M.M. Santos, M. Freitas, E. Fernandes, A comprehensive review on xanthone derivatives as α-glucosidase inhibitors, Eur. J. Med. Chem. 57 (2018) 1460–1479, https://doi.org/10.1016/j.ejmech.2018.07.073.

[23] A. Daei Farshchi Adli, R. Jahanban-Esfahlan, K. Seidi, S. Samandari-Rad, N. Zarghami, An overview on Vadimezan (DMXAA): the vascular disrupting agent, Chem. Biol. Drug Des. 91 (2018) 996–1006, https://doi.org/10.1111/cbdd.13166.

[24] M.I. Cruz, H. Cidade, M. Pinto, Dual/multitargeted xanthone derivatives for Alzheimer's disease: where do we stand? Future Med. Chem. 9 (2017) 1611–1630, https://doi.org/10.4155/fmc-2017-0086.

[25] C.A. Menéndez, B. Biscussi, S. Accordino, A.P. Murray, D.C. Gerbino, G.A. Appignanesi, Design, synthesis and biological evaluation of 1,3-dihydroxyxanthone derivatives: effective agents against acetylcholinesterase, Bioorg. Chem. 75 (2017) 201–209, https://doi.org/10.1016/j.bioorg.2017.09.012.

[26] X. Kou, L. Song, Y. Wang, Q. Yu, H. Ju, A. Yang, R. Shen, Design, synthesis and anti-Alzheimer's disease activity study of xanthone derivatives based on multi-target strategy, Bioorg. Med. Chem. Lett 30 (2020) 126927, https://doi.org/10.1016/j.bmcl.2019.126927.

[27] M. Bajda, K.J. Kuder, D. Łażewska, K. Kieć-Kononowicz, A. Więckowska, M. Ignasik, N. Guzior, J. Jończyk, B. Malawska, Dual-acting diether derivatives of piperidine and homopiperidine with histamine H(3) receptor antagonistic and anticholinesterase activity, Arch. Pharm. (Weinheim) 345 (2012) 591–597, https://doi.org/10.1002/ardp.201200018.

[28] D. Łażewska, J. Jończyk, M. Bajda, N. Szałaj, A. Więckowska, D. Panek, C. Moore, K. Kuder, B. Malawska, K. Kieć-Kononowicz, Cholinesterase inhibitory activity of chlorophenoxy derivatives-Histamine H_3 receptor ligands, Bioorg. Med. Chem. Lett 26 (2016) 4140–4145, https://doi.org/10.1016/j.bmcl.2016.04.054.

[29] Y.N. Lamb, Pitolisant: a review in narcolepsy with and without catalepsy, CNS Drugs 34 (2020) 207–218, https://doi.org/10.1007/s40263-020-00703-x.

[30] K. Wingen, H. Stark, Scaffold variations in amine warhead of histamine H_3 receptor antagonists, Drug Discov. Today Technol. 10 (2013) e483–e489, https://doi.org/10.1016/j.ddtec.2013.07.00.

[31] http://www.swissadme.ch/ (Last accessed on 5 May 2019).

[32] A.M. Waszkielewicz, K. Słoczyńska, E. Pękala, P. Żmudzki, A. Siwek, A. Gryboś, H. Marona, Design, synthesis, and anticonvulsant activity of some derivatives of xanthone with aminoalkanol moieties, Chem. Biol. Drug Des. 89 (2017) 339–352, https://doi.org/10.1111/cbdd.12842.

[33] K.J. Kuder, D. Łażewska, G. Latacz, J.S. Schwed, T. Karcz, H. Stark, J. Karolak-Wojciechowska, K. Kieć-Kononowicz, Chlorophenoxy aminoalkyl derivatives as histamine H_3R ligands and antiseizure agents, Bioorg. Med. Chem. 24 (2016) 53–72, https://doi.org/10.1016/j.bmc.2015.11.021.

[34] D. Łażewska, M. Kaleta, J.S. Schwed, T. Karcz, S. Mogilski, G. Latacz, A. Olejarz, A. Siwek, M. Kubacka, A. Lubelska, E. Honkisz, J. Handzlik, B. Filipek, H. Stark, K. Kieć-Kononowicz, Biphenyloxy-alkyl-piperidine and azepane derivatives as histamine H_3 receptor ligands, Bioorg. Med. Chem. 25 (2017) 5341–5354, https://doi.org/10.1016/j.bmc.2017.07.058.

[35] K. Sander, T. Kottke, L. Weizel, H. Stark, Kojic acid derivatives as histamine H(3) receptor ligands, Chem. Pharm. Bull. (Tokyo). 58 (2010) 1353–1361, https://doi.org/10.1248/cpb.58.135.

[36] G.L. Ellman, K.D. Courtney, V. Andres, R.M. Featherstone, A new and rapid colorimetric determination of acetylcholinesterase activity, Biochem. Pharmacol. 7 (1961) 88–95, https://doi.org/10.1016/0006-2952(61)90145-9.

[37] M. Zhou, N. Panchuk-Voloshina, A one-step fluorometric method for the continuous measurement of monoamine oxidase activity, Anal. Biochem. 253 (1997) 169–174, https://doi.org/10.1006/abio.1997.2392.

[38] T. Shimamura, M. Shiroishi, S. Weyand, H. Tsujimoto, G. Winter, V. Katritch, R. Abagyan, V. Cherezov, W. Liu, G.W. Han, T. Kobayashi, R.C. Stevens, S. Iwata, Structure of the human histamine H_1 receptor complex with doxepin, Nature 475 (2011) 65–70, https://doi.org/10.1038/nature10236.

[39] K. Szczepańska, T. Karcz, S. Mogilski, A. Siwek, K.J. Kuder, M. Kubacka Latacz, S. Hagenow, A. Lubelska, A. Olejarz, M. Kotańska, B. Sadek, H. Stark, K. Kieć-Kononowicz, Synthesis and biological activity of novel *tert*-butyl and *tert*-pentylphenoxyalkyl piperazine derivatives as histamine H_3R ligands, Eur. J. Med. Chem. 152 (2018) 223–234, https://doi.org/10.1016/j.ejmech.2018.04.043. G.

[40] A. Ballesteros, H. Weinstein, Integrated methods for the construction of three-dimensional models and computational probing of structure-function relations in G protein-coupled receptors, Methods Neurosci. 25 (1995) 366–428, https://doi.org/10.1016/S1043-9471(05)80049-7. H.

[41] K. Szczepańska, T. Karcz, A. Siwek, K.J. Kuder, G. Latacz, M. Bednarski, M. Szafarz, S. Hagenow, A. Lubelska, A. Olejarz-Maciej, M. Sobolewski, K. Mika, M. Kotańska, H. Stark, K. Kieć-Kononowicz, Structural modifications and in vitro pharmacological evaluation of 4-pyridyl-piperazine derivatives as an active and selective histamine H_3 receptor ligands, Bioorg. Chem. 91 (2019) 103071, https://doi.org/10.1016/j.bioorg.2019.103071.

[42] M. Bajda, A. Więckowska, M. Hebda, N. Guzior, C.A. Sotriffer, B. Malawska, Structure-based search for new inhibitors of cholinesterases, Int. J. Mol. Sci. 14 (2013) 5608–5632, https://doi.org/10.3390/ijms14035608.

[43] G. Kryger, I. Silman, J.L. Sussman, Structure of acetylcholinesterase complexed

with E2020 (Aricept®): implications for the design of new anti-Alzheimer drugs, Structure 7 (1999) 297–307, https://doi.org/10.1016/S0969-2126(99)80040-9.
[44] D. Łażewska, A. Olejarz-Maciej, M. Kaleta, M. Bajda, A. Siwek, T. Karcz, A. Doroz-Płonka, U. Cichoń, K. Kuder, K. Kieć-Kononowicz, 4-*tert*-Pentylphenoxyalkyl derivatives - histamine H_3 receptor ligands and monoamine oxidase B inhibitors, Bioorg. Med. Chem. Lett 28 (2018) 3596–3600, https://doi.org/10.1016/j.bmcl.2018.10.048.
[45] A.B. Salinas-Abarca, S.H. Avila-Rojas, P. Barragán-Iglesias, J.B. Pineda-Farias, V. Granados-Soto, Formalin injection produces long-lasting hypersensitivity with characteristics of neuropathic pain, Eur. J. Pharmacol. 797 (2017) 83–93, https://doi.org/10.1016/j.ejphar.2017.01.018.
[46] S. Mogilski, M. Kubacka, A. Redzicka, G. Kazek, M. Dudek, W. Malinka, B. Filipek Antinociceptive, anti-inflammatory and smooth muscle relaxant activities of the pyrrolo[3,4-d]pyridazinone derivatives: possible mechanisms of action, Pharmacol. Biochem. Behav. 133 (2015) 99–110, https://doi.org/10.1016/j.pbb.2015.03.019.
[47] D. Łażewska, M. Kaleta, S. Hagenow, S. Mogilski, G. Latacz, T. Karcz, A. Lubelska, E. Honkisz, J. Handzlik, D. Reiner, G. Satała, B. Filipek, H. Stark, K. Kieć-Kononowicz, Novel naphthyloxy derivatives - potent histamine H_3 receptor ligands. Synthesis and pharmacological evaluation, Bioorg. Med. Chem. 26 (2018) 2573–2585, https://doi.org/10.1016/j.bmc.2018.04.023.
[48] S. Mogilski, M. Kubacka, D. Łażewska, M. Więcek, M. Głuch-Lutwin, M. Tyszka-Czochara, K. Bukowska-Strakova, B. Filipek, K. Kieć-Kononowicz, Aryl-1,3,5-triazine ligands of histamine H_4 receptor attenuate inflammatory and nociceptive response to carrageen, zymosan and lipopolysaccharide, Inflamm. Res. 66 (2017) 79–95, https://doi.org/10.1007/s00011-016-0997.
[49] N. Hamzeh-Gooshchi, E. Tamaddonfard, A.A. Farshid, Effects of microinjection of histamine into the anterior cingulate cortex on pain-related behaviors induced by formalin in rats, Pharmacol. Rep. 67 (2015), https://doi.org/10.1016/j.pharep.2014.12.019, 593-9.
[50] F. Dou, X. Cao, P. Jing, C. Wu, Y. Zhang, Y. Chen, G. Zhang, Synthesis and evaluation of histamine H_3 receptor ligand based on lactam scaffold as agents for treating neuropathic pain, Bioorg. Med. Chem. Lett 29 (2019) 1492–1496, https://doi.org/10.1016/j.bmcl.2019.04.015.
[51] K. Sałat, M. Kołaczkowski, A. Furgała, A. Rojek, J. Śniecikowska, M.A. Varney, A. Newman-Tancredi, Antinociceptive, antiallodynic and antihyperalgesic effects of the 5-HT_{1A} receptor selective agonist, NLX-112 in mouse models of pain, Neuropharmacology 125 (2017) 181–188, https://doi.org/10.1016/j.neuropharm.2017.07.022.
[52] A. Alachkar, N. Khan, D. Łażewska, K. Kieć-Kononowicz, B. Sadek, Histamine H_3 receptor antagonist E177 attenuates amnesia induced by dizocilpine without modulation of anxiety-like behaviors in rats, Neuropsychiatric Dis. Treat. 15 (2019) 531–542, https://doi.org/10.2147/NDT.S193125.
[53] A. Alachkar, D. Łażewska, K. Kieć-Kononowicz, B. Sadek, The histamine H_3 receptor antagonist E159 reverses memory deficits induced by dizocilpine in passive avoidance and novel object recognition paradigm in rats, Front. Pharmacol. 8 (2017) 709, https://doi.org/10.3389/fphar.2017.00709.
[54] N. Eissa, N. Khan, S.K. Ojha, D. Łażewska, K. Kieć-Kononowicz, B. Sadek, The histamine H_3 receptor antagonist DL77 ameliorates MK801-induced memory deficits in rats, Front. Neurosci. 12 (2018) 42, https://doi.org/10.3389/fnins.2018.00042.
[55] B. Sadek, A. Saad, D. Subramanian, M. Shafiullah, D. Łażewska, K. Kieć-Kononowicz, Anticonvulsant and procognitive properties of the non-imidazole histamine H_3 receptor antagonist DL77 in male adult rats, Neuropharmacology 106 (2016) 46–55, https://doi.org/10.1016/j.neuropharm.2015.10.023. B.
[56] B. Sadek, N. Khan, F.H. Darras, S. Pockes, M. Decker, The dual-acting AChE inhibitor and H_3 receptor antagonist UW-MD-72 reverses amnesia induced by scopolamine or dizocilpine in passive avoidance paradigm in rats, Physiol. Behav. 165 (2016) 383–391, https://doi.org/10.1016/j.physbeh.2016.08.022.
[57] A. Alachkar, S. Azimullah, M. Lotfy M, E. Adeghate, S.K. Ojha, R. Beiram, D. Łażewska, K. Kieć-Kononowicz, B. Sadek, Antagonism of histamine H_3 receptors alleviates pentylenetetrazole-induced kindling and associated memory deficits by mitigating oxidative stress, central neurotransmitters, and c-Fos protein expression in rats, Molecules 25 (2020) 1575, https://doi.org/10.3390/molecules25071575.
[58] A. Alachkar, S.K. Ojha, A. Sadeq, A. Adem, A. Frank, H. Stark, B. Sadek, Experimental models for discovery of novel anticonvulsant drugs: focus on pentylenetetrazole-induced seizures and associated memory deficits, Curr. Pharmaceut. Des. 26 (2020) 1693–1711, https://doi.org/10.2174/1381612826666200131105324.
[59] A. Diana, O. Michielin, Y. Zoete, Swiss ADME: a free web tool to evaluate pharmacokinetics, drug-likeness and medicinal chemistry friendliness of small molecules, Sci. Rep. 7 (2017) 42717, https://doi.org/10.1038/srep42717.
[60] http://tox.charite.de/protox_II/ (last access February 2020).
[61] G. Latacz, A. Lubelska, M. Jastrzębska-Więsek, A. Partyka, M.A. Marć, G. Satała, D. Wilczyńska, M. Kotańska, M. Więcek, K. Kamińska, A. Wesołowska, K. Kieć-Kononowicz, J. Handzlik, The 1,3,5-triazine derivatives as innovative chemical family of 5-HT_6 serotonin receptor agents with therapeutic perspectives for cognitive impairment, Int. J. Mol. Sci. 20 (2019) 1–21, https://doi.org/10.3390/ijms20143420.
[62] X. Chen, A. Murawski, K. Patel, C.L. Crespi, P.V. Balimane, A novel design of artificial membrane for improving the PAMPA model, Pharm. Res. (N. Y.) 25 (2008) 1511–1520, https://doi.org/10.1007/s11095-007-9517-8.
[63] R.A. Finnegan, P.L. Bachman, Natural occurrence of 2-hydroxyxanthone, J. Pharmacol. Sci. 54 (1965) 633–635, https://doi.org/10.1002/jps.2600540431.
[64] Y.C. Cheng, W. Prusoff, Relationship between the inhibition constant (KI) and the concentration of inhibitor which causes 50 per cent inhibition (I50) of an enzymatic reaction, Biochem. Pharmacol. 22 (1973) 3099–3108, https://doi.org/10.1016/0006-2952(73)90196-2.
[65] Schrödinger Release 2018-1, Schrödinger Suite 2018-1 Protein Preparation Wizard, Epik, Schrödinger, LLC, New York, NY, 2018.
[66] Schrödinger Release 2018-1, ConfGen, Schrödinger, LLC, New York, NY, 2018.
[67] K.S. Watts, P. Dalal, R.B. Murphy, W. Sherman, R.A. Friesner, J.C. Shelley, ConfGen: a conformational search method for efficient generation of bioactive conformers, J. Chem. Inf. Model. 50 (2010) 534–546, https://doi.org/10.1021/ci100015j.
[68] Schrödinger Release 2018-1, Glide, Schrödinger, LLC, New York, NY, 2018.
[69] T.A. Halgren, R.B. Murphy, R.A. Friesner, H.S. Beard, L.L. Frye, W.T. Pollard, J.L. Banks, Glide: a new approach for rapid, accurate docking and scoring. 2. Enrichment factors in database screening, J. Med. Chem. 47 (2004) 1750–1759, https://doi.org/10.1021/jm030644s.
[70] R.A. Friesner, R.B. Murphy, M.P. Repasky, L.L. Frye, J.R. Greenwood, T.A. Halgren, P.C. Sanschagrin, D.T. Mainz, Extra precision glide: docking and scoring incorporating a model of hydrophobic enclosure for protein-ligand complexes, J. Med. Chem. 49 (2006) 6177–6196, https://doi.org/10.1021/jm051256o.
[71] E.F. Pettersen, T.D. Goddard, C.C. Huang, G.S. Couch, D.M. Greenblatt, E.C. Meng, T.E. Ferrin, UCSF Chimera–a visualization system for exploratory research and analysis, J. Comput. Chem. 25 (2004) 1605–1612, https://doi.org/10.1002/jcc.20084.
[72] K. Socała, M. Mogilski, M. Pieróg, D. Nieoczym, M. Abram, B. Szulczyk, A. Lubelska, G. Latacz, U. Doboszewska, P. Wlaź, K. Kamiński, KA-11, a novel pyrrolidine-2,5-dione derived broad-spectrum anticonvulsant: its anti-epileptogenic, antinociceptive properties and in vitro characterization, ACS Chem. Neurosci. 10 (2019) 636–648, https://doi.org/10.1021/acschemneuro.8b00476.
[73] N. Eissa, P. Jayaprakash, S. Azimullah, S.K. Ojha, M. Al-Houqani, F.Y. Jalal, D. Łażewska, K. Kieć-Kononowicz, B. Sadek, The histamine H_3R antagonist DL77 attenuates autistic behaviors in a prenatal valproic acid-induced mouse model of autism, Sci. Rep. 8 (2018) 13077, https://doi.org/10.1038/s41598-018-31385-7.
[74] N. Eissa, S. Azimullah, P. Jayaprakash, R.L. Jayaraj, D. Reiner, S.K. Ojha, R. Beiram, H. Stark, D. Łażewska, K. Kieć-Kononowicz, B. Sadek, The dual-active histamine H_3 receptor antagonist and acetylcholine esterase inhibitor E100 ameliorates stereotyped repetitive behavior and neuroinflammmation in sodium valproate induced autism in mice, Chem. Biol. Interact. 312 (2019) 108775, https://doi.org/10.1016/j.cbi.2019.108775.
[75] G. Latacz, A. Lubelska, M. Jastrzębska-Więsek, A. Partyka, A. Sobilo, A. Olejarz, K. Kucwaj-Brysz, G. Satała, A.J. Bojarski, A. Wesołowska, K. Kieć-Kononowicz, J. Handzlik, In the search for a lead structure among series of potent and selective hydantoin 5-HT_7R agents: the drug-likeness in vitro study, Chem. Biol. Drug Des. 90 (2017) 1295–1306, https://doi.org/10.1111/cbdd.13106.